



저작자표시-변경금지 2.0 대한민국

이용자는 아래의 조건을 따르는 경우에 한하여 자유롭게

- 이 저작물을 복제, 배포, 전송, 전시, 공연 및 방송할 수 있습니다.
- 이 저작물을 영리 목적으로 이용할 수 있습니다.

다음과 같은 조건을 따라야 합니다:



저작자표시. 귀하는 원저작자를 표시하여야 합니다.




변경금지. 귀하는 이 저작물을 개작, 변형 또는 가공할 수 없습니다.

- 귀하는, 이 저작물의 재이용이나 배포의 경우, 이 저작물에 적용된 이용허락조건을 명확하게 나타내어야 합니다.
- 저작권자로부터 별도의 허가를 받으면 이러한 조건들은 적용되지 않습니다.

저작권법에 따른 이용자의 권리는 위의 내용에 의하여 영향을 받지 않습니다.

이것은 [이용허락규약\(Legal Code\)](#)을 이해하기 쉽게 요약한 것입니다.

[Disclaimer](#) 

이학석사 학위논문

**Development of cationic
pH-responsive albumin binding
ligands with enhanced blood half-life
for the cancer theranostics**

암 표적 테라노스틱스를 위한 강화된 혈중
반감기를 보이는 양이온성 pH 반응성
알부민 결합 리간드의 개발

2023년 2월

서울대학교 융합과학기술대학원

응용바이오횡학과

이 정 섭

**Development of cationic
pH-responsive albumin binding
ligands with enhanced blood half-life
for the cancer theranostics**

지도교수 임 형 준

이 논문을 이학석사 학위논문으로 제출함
2023년 1월

서울대학교 융합과학기술대학원
응용바이오공학과 응용바이오공학전공
이 정 섭

이정섭의 이학석사 학위논문을 인준함
2023년 1월

위 원 장 _____ 이 강 원 _____ (인)
부위원장 _____ 임 형 준 _____ (인)
위 원 _____ 이 병 철 _____ (인)

Abstract

Development of cationic pH-responsive albumin binding ligands with enhanced blood half-life for the cancer theranostics

Jeong-Seob Lee

Department of Applied Bioengineering

The Graduate School of Convergence Science and Technology

Seoul National University

Albumin is the most abundant protein in human plasma, has a long circulation half-life (19 days), and transports various molecules through the circulatory system. Therefore, the circulation time and tissue targeting ability of a drug can be enhanced by adding albumin-binding motif to the drug. Herein, we developed a pH-responsive albumin-binding ligand (ABL-His) that consists of a fatty acid-based binding moiety and an imidazole moiety in histidine for charge-exchangeable property at low pH conditions, resulting in reduced interaction with albumin to be detached. We hypothesized that our pH-responsive ABL-His has enhanced tumor targeting ability due to its ability to 1) bind serum albumin reversibly and 2) be released in the low pH tumor microenvironment. By introducing RITC (rhodamine B isothiocyanate) as a fluorescence dye, ABLs suggest that it has a great potential to be utilized for drug delivery platforms for achieving effective tumor targeted imaging and therapy. Synthesized RITC-ABL-His and -Gly (non pH-responsive ABL) presented more than 2-fold higher albumin

binding capacity (48.3, 45.6% respectively) compared to free RITC (20.2%). Furthermore, RITC-ABL-His showed reduced albumin-binding capacity due to the reduced interaction with albumin resulting from charge-exchange of imidazole at low pH conditions. In vitro study, we confirmed that RITC-ABLs showed the high fluorescent intensity within CT26 cancer cells at neutral pH. Through in vivo and ex vivo fluorescence imaging in CT26 tumor bearing-mice, tumor uptake of RITC-ABL-His group was significantly higher than that of the other two groups (RITC-ABL-Gly and RITC). Considering these studies, RITC labeled ABLs showed a potential as a cancer imaging agent. In accordance with the superior targeting property of ABL-His, we prepared IR780-ABL-His by immobilizing IR780 which is a near-infrared light activatable photosensitizer on the ABLs. The physicochemical characteristics of IR780-ABL-His have been evaluating with 808-nm laser irradiation for application to photodynamic/photothermal therapy as well. In conclusion, the ABLs can show great potential as an cancer targeted imaging probe or anticancer agents. Therefore, we anticipate that the pH-responsive ABLs will be effective anticancer drug platforms by introducing radionuclide and photosensitizers based on their extended circulation and pH-responsive tumor-targeting ability as cancer targeted imaging/therapy agents.

keywords: albumin, fatty acid, blood half-life, pH-responsive drug delivery, fluorescence imaging, photodynamic therapy

Student Number: 2021-26205

Contents

Chapter 1. Introduction

1.1 Albumin as bioactive molecules transporter	1
1.2 pH-responsive drug delivery	6
1.3 Aim of this study	8

Chapter 2. Experimental

2.1 General experimental section	11
2.2 Synthesis of RITC-ABLs	12
2.3 Synthesis of IR780-ABLs	17
2.4 Synthesis of [⁶⁴ Cu]DOTA-ABLs	20
2.5. In vitro evaluation of RITC-ABLs	22
2.6 In vivo/ex vivo evaluation of RITC-ABLs	26

Chapter 3. Result and discussion

3.1 Chemistry of the albumin binding ligands.	28
3.2 In vitro imaging and cellular uptake of RITC-ABLs	32
3.3 In vivo and ex vivo optical imaging of RITC-ABLs	35

Chapter 4. Conclusion

Appendix	42
----------------	----

Reference	43
-----------------	----

Abstract in Korean	48
--------------------------	----

Figure legends

Figure 1.1. Crystal structural illustration of human serum albumin (reproduced from Vicente A et al. [1]).

Figure 1.2. Schematic illustration of three types of fatty acid. Short-chain FAs (SCFAs), medium-chain FA (MCFAs) and long-chain FAs (LCFAs) (reproduced from Vicente A et al [2]).

Figure 1.3. Potential stimuli and responses in stimuli-responsive drug delivery system (reproduced from Malekmohammadi S. et al. [3]).

Figure 1.4. Distinct pH level as a biomarker in each organ, tissue and cellular levels and their potential application (reproduced from Bazban-Shotorbani. et al.[4]).

Figure 1.5. Schematic figure of hypothesized working mechanism of RITC-ABL-His.

Figure 1.6. Library of albumin binding ligands for imaging and therapy. RITC-ABL-His (1), RITC-ABL-Gly (2) for fluorescence imaging. IR780-ABL-His (3) and IR780-ABL-Gly (4) for NIR fluorescence imaging and photodynamic therapy.

Figure 2.1 Synthetic scheme of RITC-ABL-His and RITC-ABL-Gly.

Figure. 2.2 Synthesis of IR780-NCS. Reagent and conditions: (i) 4-aminthiophenol, DMF, 25 °C, 24 h; (ii) di(2-pyridyl)thionocarbonate, DCM, 25 °C, 12h.

Figure 2.3. Synthesis of IR780-ABL-His (3) and IR780-ABL-Gly (4). Reagent and conditions: (i) IR780-NCS, TEA, DMF, 85 °C, 1 h.

Figure 2.4 Synthesis of DOTA-ABL-His (5') and DOTA-ABL-Gly (6'). Reagent and conditions: (i) (p-SCN-Bn)-DOTA, TEA, DMF, 85 °C, 1 h

Figure 1.5 Radiosynthesis of [⁶⁴Cu]DOTA-ABL-His (5) and [⁶⁴Cu]DOTA-ABL-

Gly (6). Reagent and conditions: (i) [^{64}Cu]CuCl₂, water, 80 °C, 30 min

Figure 3.1 (A) UV/Vis absorption spectra and (B) emission spectra of RITC-ABL-His, RITC-ABL-Gly and RITC (Each 1.6 μM). Similar absorption and emission properties among three molecules was confirmed to have similar absorption maxima at $\lambda \approx 550$ nm and emission maxima at $\lambda \approx 570$ nm.

Figure 3.2 Molecular docking simulation of RITC-ABL-His with human serum albumin under different pH level (pH 7.4, 6.5 and 5.5). It demonstrates the interaction between RITC-ABL-His and HSA. Hydrogen bond (green), covalent bond (pink), and non-covalent bond (Red).

Figure 3.3 (A) Binding profiles with BSA was examined by using size exclusion chromatography method. The RITC-ABLs attached to albumin more than twice as much as free RITC in neutral pH. (B) Released RITC-ABLs from albumin under acidic condition was measured. pH-responsive RITC-ABL-His was identified to have reduced binding efficacy with albumin as the pH decreased from 7.4 to 5.5. RITC-ABL-Gly showed no difference in all range of pH. (ns = not significant $p \geq 0.05$, * $P < 0.05$, ** $p < 0.01$, *** $p < 0.001$)

Figure 3.4 In vitro cellular uptake of CT26 cancer cells was observed, 15 μmol of RITC-ABL-His and RITC-ABL-Gly treated CT26 cells at all the various time points (0, 0.5, 2, 24 and 48 h).

Figure 3.5 Representative in vivo and ex vivo fluorescence images of RITC-ABL-His, RITC-ABL-Gly and RITC in CT26 tumor bearing mouse model at 0, 2, 8, 24 h post injection (n=4). (Tu: tumor, Sp: spleen, Li: liver, He: heart, Ki: kidney, Lu: lung..

Figure 3.6 Quantitative analysis of ex vivo images of RITC-ABL-His, RITC-ABL-Gly and RITC in CT26 tumor bearing mouse model (n=3) at 24 h after intravenous

injection of the fluorescence probes and tumor targeting efficiency compared to five normal organs. (A) Biodistribution analysis of various organs and tumors. (B) Tumor to normal organ ratio (B) liver, (C) heart, (D) spleen, (E) kidney, (F) lung (** $p < 0.01$)

Table legends

Table 1. Albumin binding proteins and receptors and its expression localization and their substrate [5, 6]

Table 2. Evaluated binding free energy of the RITC-ABL-His under three distinct pH condition (pH 7.4, 6.5 and 5.5)

Chapter 1. Introduction

1.1 Albumin as bioactive molecules transporter

Albumin (molecular weight of 66.5 kDa) is the most abundant protein (35-50 g/L human serum) in human plasma and has an extraordinarily long blood circulation half-life (~19 days) [7]. It is produced as pre-proalbumin in the liver and secreted from the hepatocytes after being matured in the reticulum [8, 9]. Albumin is heart shaped molecule with 585 residues and three main domains containing two sub-domains. Structure of albumin mainly consist of three main domains each has two subdomains. There are several binding sites of fatty acid that located across the whole body of albumin [1].

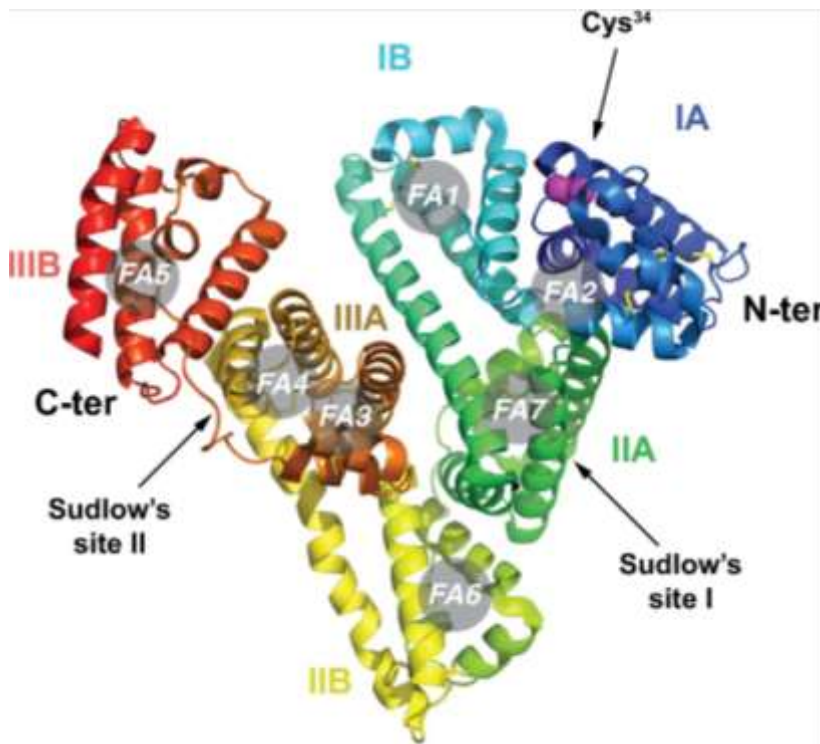


Figure 2.1. Crystal structural illustration of human serum albumin (reproduced from Vicente A et al. [1])

Long half-life is occurred by several factors such as neonatal Fc receptor (FcRn)-mediated recycling [1]. Moreover, it is well known to transport a variety of essential substances including ligands, metal ions and therapeutic drug through the circulatory system [10-12]. Therefore, albumin can play important roles in drug delivery because of its intrinsic ability to transport ligands and its exquisite properties such as high solubility, stability and low immunogenicity [3, 12, 13].

A lot of albumin binding drugs and imaging probes were already reported. For example, Gadofosveset [14], Evans blue [15, 16] and ICG [17] so on were known as albumin binding probes and anti-cancer agent like Paclitaxel [13, 18, 19], Camptothecin [20], Gemcitabine [21], etc were already proved to be bound to albumin.

There are two tumor internalization mechanisms of albumin: the enhanced permeability and retention (EPR) effect and protein/receptor-mediated tumor accumulation and catabolism [18]. First, vascular permeability enhancing factors which are the mediators of tumor-associated vascular hyperpermeability like nitric oxide increases microvascular permeability in solid tumors [22, 23]. Vascular hyperpermeability leads to the enhanced permeation and retention effect called EPR effect that induces higher uptake and accumulation within the tumor interstitium of macromolecules which have larger molecular weight more than 40 kDa [5]. Enhanced accumulation of those albumin-bound drugs in tumors was turned out previously that it was given a rise to EPR effect of albumin, resulting from improved vascular permeability and avoided lymphatic drainage [18, 24]. Moreover, albumin exhibits reduced clearance from tumor due to its high molecular weight. Circulating half-life is one of the most important parameters in drug development and pharmacology because therapeutic effect can be decreased if

drugs show rapid clearance after they were administered [25].

Second, several albumin binding protein or receptor-mediated accumulations of albumin have been studied besides EPR effect. Receptor-mediated albumin uptake pathways are occurred in some cancer cells [26], and they have additional advantages in tumor uptake into the interstitium among several tumor tissue.

Protein/Receptor	Tissue/Cells	Substrate
Albondin/gp60	Endothelial cells	Native albumin
gp18	Endothelium, macrophages and a range of cancer	Modified-albumin
gp30	Endothelium, macrophages, fibroblast and breast cancer	Modified-albumin
hnRNPs	Breast cancer, melanoma cells	Native albumin
Calreticulin	Breast cancer, melanoma cells, kidneys, intestinal cells, placenta	Native albumin
FcRn	Endothelium, gut, liver, kidneys, lungs	Native albumin
Cubilin	Small intestine, placenta, kidneys	Native albumin/modified-albumin
Megalin	Thyocytes, choroid plexus, proximal tubule cells	Native albumin/modified-albumin
CD36	Macrophages, kidneys	Modified albumin
SPARC	Endothelial cells, vascular smooth muscle cells, skeletal muscle, fibroblast, testicular, ovarian, pancreatic tumor cells	Native albumin

Table 2. Albumin binding proteins and receptors and its expression localization and their substrate [5, 6].

For example, one of the intracellular receptors like Neonatal Fc receptor (FcRn)-mediated endogenous transportation of molecules like fatty acids with albumin engagement are well reported [27]. It contributes to long blood half-life of albumin by interacting with albumin strongly and preventing albumin from lysosomal degradation as it undergoes endocytosis under endosomal pH (6-6.5) [18, 26, 28]. After that the FcRn-bound albumin could be released back to the interstitium [18, 29].

Considering these points, albumin can be used as not only a non-covalently binding drug carrier, but as a backbone of covalently drug-conjugated albumin nano-drug on its surface of each domains to maximize advantages of albumin in tumor targeted imaging and therapy by EPR effect as well as protein/receptor-

mediated pathways [10]. For these reasons, albumin has great potentials to be developed as emerging drug delivery carrier platform in two ways, 1) Non-covalently albumin binding drugs 2) Covalently drug albumin conjugation. Both strategies are extensively under investigation. We focused on the former strategy to develop a long blood circulating probe by introducing fatty acid (FA) as a non-covalently binding motif to albumin.

Fatty acids (FAs) are naturally occurring in the body and albumin is the major carrier of them under physiological condition. Many analyses about FA-albumin binding sites were addressed that binding sites mainly contain hydrophobic branched residues such as leucine, valine, and isoleucine because of inter-molecular interactions among FA and albumin [12].

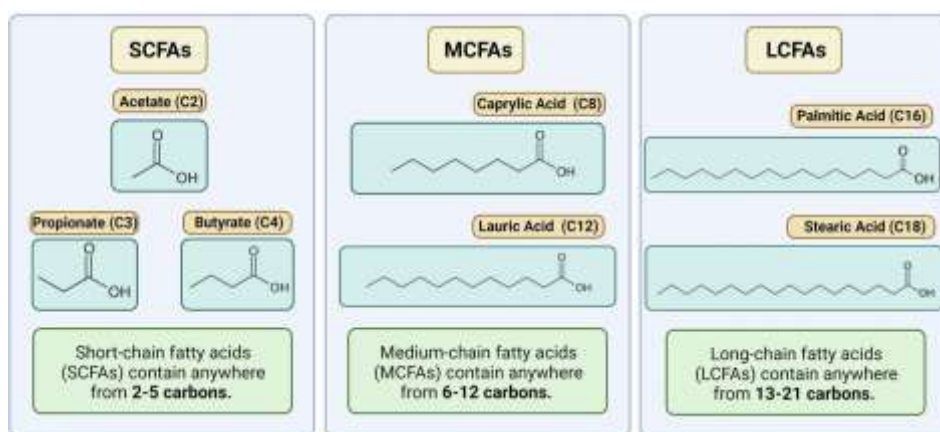


Figure 1.2. Schematic illustration of three types of fatty acid. Short-chain FAs (SCFAs), medium-chain FA (MCFAs) and long-chain FAs (LCFAs). (reproduced from Vicente A et al [2].)

Since immobilization of FAs on endogenous and exogenous ligands has been revealed to delay their rapid clearance and reduce immunogenicity of the drug

molecules, FA can be a good choice as a albumin binder to improve blood half-life of ligands. Bovine serum albumin and human serum albumin have seven binding sites for fatty acid. FAs are major sources of lipids in metabolic system [30]. Even long chain fatty acids are hydrophobic and have low solubility in physiological conditions, albumin solubilize them stable in the body system. That's why FA-conjugation on drugs can play important roles as an effective drug delivery [10]. Furthermore, binding affinity of FA depending on their length were reported. Short-to medium length FAs (8 to 12 carbons) bind has with KD values between 0.5 and 60 μM [12]. We utilized decanoic acid which is consisted of 10 carbons and binding constant (KD) of it was measured as $8.42 \pm 0.4 \mu\text{M}$ [31]. Unique property of fatty acid derivatives to bind to albumin through several binding sites in albumin is one of the main reasons that fatty acids were used as a albumin binder [3]. In this study, introducing decanoic acid as a albumin binder to device albumin binding ligand to endows improved blood circulation profile and selective ligand releasing effect in tumor microenvironment. Several successful examples of drugs including Levemir[®], Saxenda[®], Ozempic[®], Tresiba[®] were approved that used non-covalent albumin binding to extend blood circulation half-life [32].

Using fatty acid as a albumin binder in polymer and peptide for the enhanced drug delivery is common, however there remains a need for improvement of specific tumor targeting abilities in case of cancer therapies. In order to increase tumor targeting efficacy, we need to add additional functionalities like tumor targeting moiety which has active targeting or passive targeting ability.

1.2 pH-responsive drug delivery

There are a lot of exogenous and endogenous stimuli to be utilized for the targeted delivery. Stimuli-responsive drug delivery system has been widely adopted to grant drugs precise targeting ability in various drugs (**figure 1.3**).

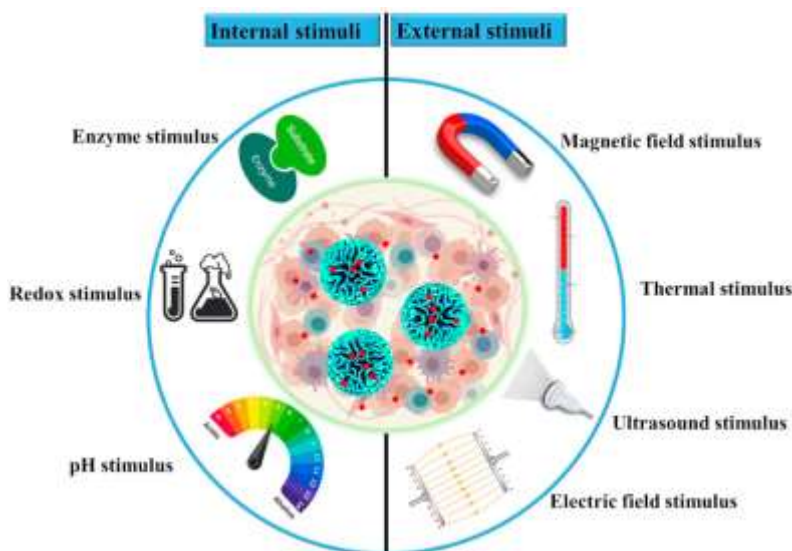


Figure 1.3. Potential stimuli and responses in stimuli-responsive drug delivery system (reproduced from Malekmohammadi S. et al. [3])

As shown in **figure 1.4**, distinct tissue has different pH condition to maintain their own roles. Especially in case of tumor, pH differences between cancerous and healthy tissues are common, and it can be exploited to make pH-responsive, tumor-targeted drug delivery.

Currently, many studies still have being reported their trials to utilized pH as potential stimuli in drug delivery system to achieve specifically high local drug concentrations in tumors. That's because most of the tumor tissue has low pH level in tumor microenvironments that caused by accumulation of lactic acid during rapid growth in tumor cells [33]. Microenvironment in human tumors has lower pH

states than that of in normal organs in range of 5.7-7.8 [34].

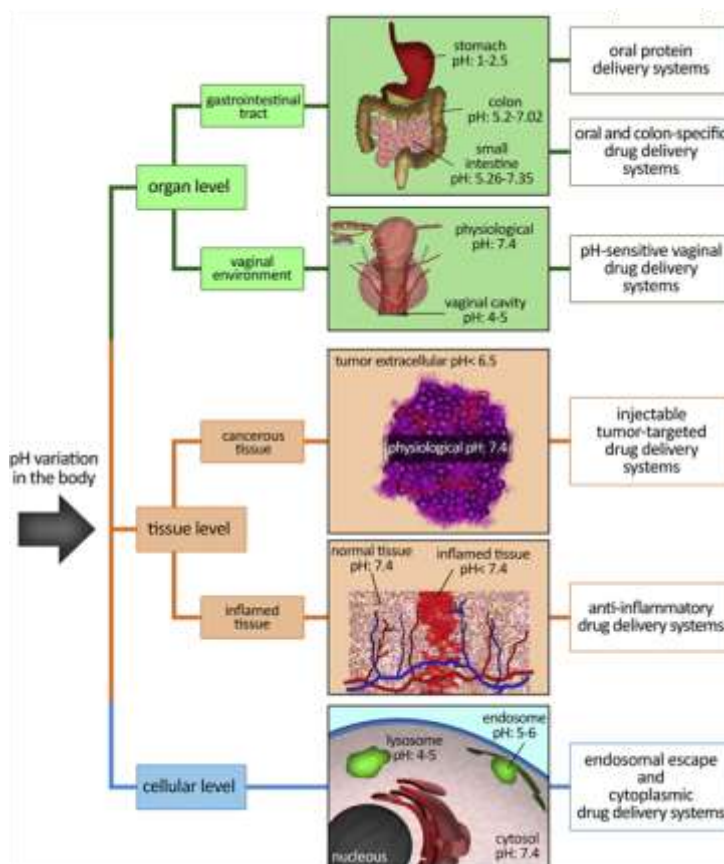


Figure 1.4. Distinct pH level as a biomarker in each organ, tissue and cellular levels and their potential application (reproduced from Bazban-Shotorbani. et al.[4]).

In order to have specific release profile at tumor tissue, drug was added by functionalization of a pH-responsive moiety in the ligand for the improvement of its pharmacological profile. To improve tumor uptake of our ligands, we adopted pH as a stimuli to response with. That's because tumor microenvironment (TME) usually have lower pH than that of normal cell microenvironment [35]. Especially in solid tumor, concentration of H^+ is significantly higher than others owing to their

fast catabolism and lots of proton as an energy resource.

Changes in the pH conditions, these aspects of solid tumor make pH-responsive drug delivery more attractive. To realize pH responsive nanoparticles, anionic or cationic polymers have been employed as pH responsive functionalities in many prior studies. Structure of albumin is stable in a range of pH 4.0 pH 9.0 though changes in shape could be occurred [36].

In order to develop the cancer theranostic agents with

1.3 Aim of this study

It is especially notable that protonation effect by pH variations can trigger different pharmacokinetics in physiological conditions. Though pH responsive moiety usually applied in polymer science, we designed a simple molecule that contains imidazole functional groups that can be protonated in low pH as well as albumin binding moiety. We expected imidazole containing albumin binding ligand, named as RITC-ABL-His will show exquisite potentials as an effective tumor targeted fluorescence probe.

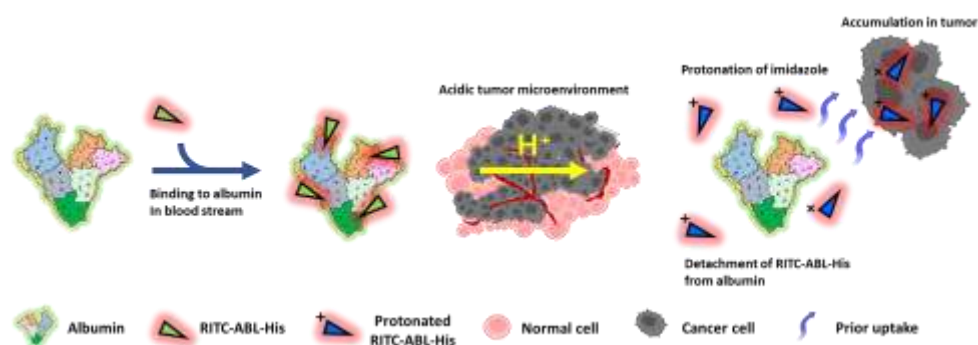


Figure 1.5. Schematic figure of hypothesized working mechanism of RITC-ABL-His.

To sum up, the circulation time and tissue targeting ability of a drug can be enhanced by adding albumin binding motif to the drug. Herein, we developed the pH-responsive albumin-binding ligand that is consist of fatty acid-based albumin binding motif and an imidazole moiety. The imidazole moiety can be protonated at low pH conditions, resulting in reduced interaction with albumin (**figure 1.5**).

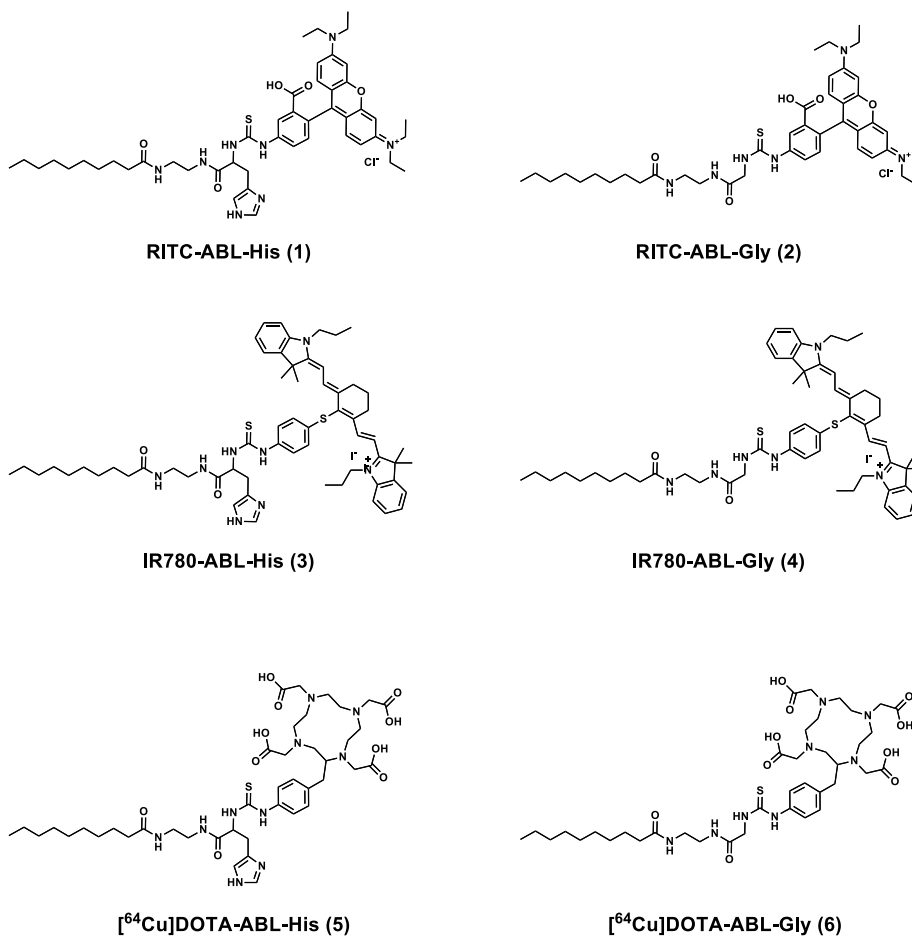


Figure 1.6 Library of albumin binding ligands for imaging and therapy. RITC-ABL-His (1), RITC-ABL-Gly (2) for fluorescence imaging. IR780-ABL-His (3) and IR780-ABL-Gly (4) for NIR fluorescence imaging and photodynamic therapy. [⁶⁴Cu]DOTA-ABL-His (5) and [⁶⁴Cu]DOTA-ABL-Gly (6) for nuclear imaging and therapy

We hypothesized that our pH-responsive albumin-binding ligand has enhanced tumor targeting ability due to its ability to 1) bind serum albumin and 2) be released at low pH conditions in tumor tissues. And its improved pharmacokinetics and diagnostic/clinical efficacy can be applied as delivery system for the generation of therapeutics. The ABLs has many advantages that 1) it is easy and cheap to synthesize, 2) we can facilitate this platform by substitution of other FA or pH responsive functionalities. Structures of the designed albumin binding ligands are shown in **figure 1.6**.

Chapter 2. Experimental

2.1 General experimental section

Commercial reagent grade chemicals were used without further purification. Ethylenediamine was purchased from Sigma-Aldrich Corp. (St. Louis, MO, UA). Di-tert-butyl dicarbonate, decanoic acid, N-(tert-Butoxycarbonyl)glycine, N^α-(tert-Butoxycarbonyl)-L-histidine was obtained from Tokyo Chemical Industry (Tokyo, Japan) Flash column chromatography was conducted using silica gel (Merck, 230-400 mesh, ASTM). All reaction was monitored by thin layer chromatography (Merck, silica gel 60F254). Size exclusion PD-10 column and fetal bovine serum (FBS) were obtained from GE Healthcare Life Science (Buckinghamshire, UK). Electrospray mass spectrometry (ESI-MS) was performed on an Agilent 1100 LC-MSD trap system instrument (Palo Alto, CA, USA). ¹H and ¹³C NMR spectra were obtained by Varian 400-MR spectrometer (Agilent) at ambient conditions and deuterated solvents such as CDCl₃, DMSO, MeOD. Chemical shifts were reported in parts per million (ppm, δ units). Absorbance and fluorescence were measured by a microplate reader (SYNERGY H1, BioTek, Winooski, VT, USA). A confocal microscopy (Nikon A1R, Nikon Co., Tokyo, Japan) was operated to observe cellular uptake. In vivo mice fluorescence images were obtained using in vivo imaging system (IVIS, IVIS Lumina X5 Imaging System, Perkin-Elmer, Waltham, MA, U.S). Human albumin and bovine serum albumin were purchased from Sigma-Aldrich (St. Louis, MO, USA). 4% paraformaldehyde (PFA) was purchased from Biosesang (Seongnam, Korea). ViaFluor[®] 488 Live Cell Microtubule Staining Kit was acquired from Biotuim (Fremont, CA, USA). All cell experiments were performed with culture medium; Dulbecco's modified Eagle medium (DMEM),

10% fetal bovine serum (FBS), and 1% penicillin-streptomycin (PS) were purchased from Hyclone (Utah, USA). For living cell fluorescence labeling, nuclei and microtubules were stained with Hoechst 33342 (Invitrogen, Carlsbad, USA) and ViaFluor[®] 488 (Biotium, California, USA) respectively. All animal experiments were performed with the approved (No.) of the IACUC2003-036-01. Female BALB/c nude mice (6–8 weeks) were obtained from Orient Bio (Seongnam, Korea) for in vivo Biodistribution of ABL Statistical analysis is expressed as the mean \pm standard deviation of the mean. Analysis was performed with SigmaPlot (version 10.0)

2.2 Synthesis of RITC-ABLs

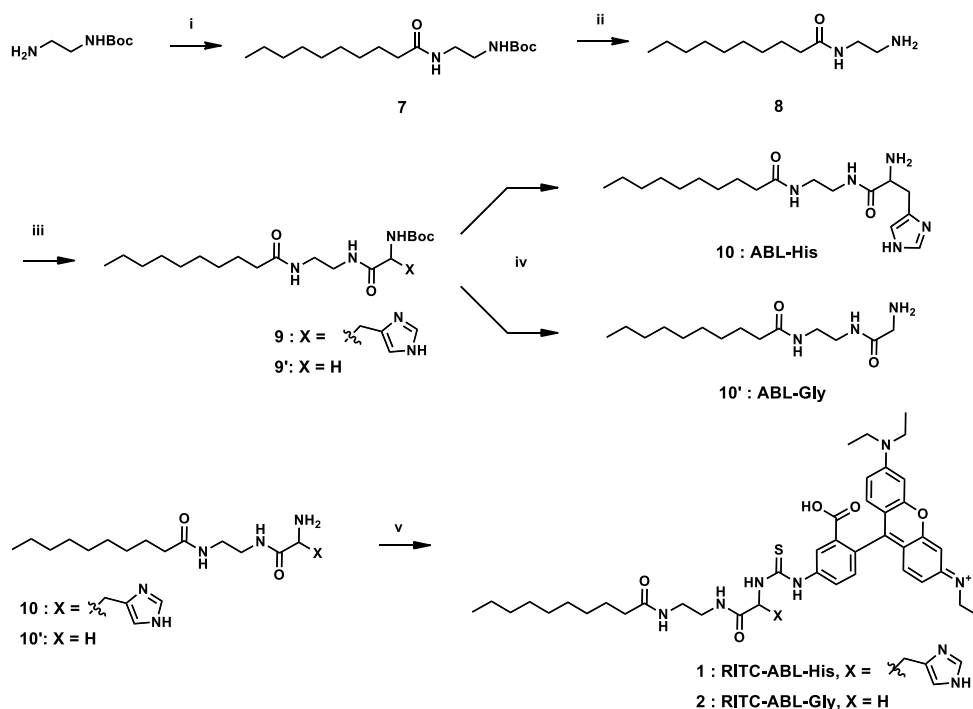


Figure 2.1 Synthetic scheme of RITC-ABL-His and RITC-ABL-Gly

Synthesis of *tert*-butyl (2-decanamidoethyl)carbamate (ABL-NHBoc, 7)

A mixture of decanoic acid (1 g, 5.8054 mmol), benzotriazol-1-yloxytris(dimethylamino)phosphonium hexafluorophosphate (BOP, 2.5675 g, 5.8051 mmol) in anhydrous dichloromethane (DCM, 40 mL) was stirred at room temperature for 30 minutes. After adding of N, N'-diisopropylethylamine (1.7258 g, 13.352 mmol), the reaction mixture was for 18 hours. After that, the solvent was removed under reduced pressure and the mixture was extracted with a solution of 1 M potassium hydrogen sulfate (30 mL) and dichloromethane (3×30 mL). The extracted organic layer was dried over anhydrous Na₂SO₄ and evaporated under reduced pressure. The crude product was purified by silica gel column chromatography using 10% Methanol-Dichloromethane as the eluent, to afford as a white solid (1.71 g, 93.5%) ¹H NMR (400 MHz, CDCl₃) δ 6.15 (s, 1H), 4.92 (s, 1H), 3.43 (t, J = 6.1 Hz, 2H), 3.32-3.29 (m, 2H), 2.16 (t, J = 7.0 Hz, 2H), 1.66-1.54 (m, 2H), 1.44 (s, 9H), 1.25 (m, 12H), 0.87 (t, J = 6.9 Hz, 3H).

Synthesis of *N*-(2-aminoethyl)decanamide (ABL-NH₂ 8)

In a dry flask equipped with a stirring bar, the ABL-NHBoc **7** (600 mg, 1.908 mmol) was dissolved in 1:1 v/v mixture of TFA/DCM (6 mL) and allowed to stir at room temperature for 5 hours. The reaction was monitored via TLC. Upon complete conversion of the N-Boc-protected amine to primary amine, saturated NaHCO₃ (50 mL) was added to the resulting solution and the whole was extracted with dichloromethane (20×3 mL). Combined organic extracts were dried over Na₂SO₄ and concentrated to give the ABL-NH₂ **8** (407 g, 99%) as yellowish oil. ¹H NMR (400 MHz, MeOD), δ 3.43 (t, J = 6.1 Hz, 2H), 3.03 (t, J = 6.0 Hz, 2H), 2.13 (t, J = 7.8 Hz, 2H), 1.64 – 1.55 (m, 2H), 1.35 – 1.25 (m, 12H), 0.89 (t, J = 6.9 Hz, 3H).

Synthesis of *tert*-butyl (1-((2-decanamidoethyl)amino)-3-(1H-imidazol-4-yl)-1-oxopropan-2-yl)carbamate (ABL-His-NHBoc, 9)

A mixture of ABL-NH₂ **8** (800 mg, 3.7 mmol), Na-(*tert*-Butoxycarbonyl)-L-histidine (953 mg, 3.7 mmol), and benzotriazol-1-yloxytris(dimethylamino)phosphonium hexafluorophosphate (BOP, 1.65 g, 3.7 mmol) in anhydrous dichloromethane (DCM, 40 mL) was stirred at room temperature for 30 minutes. After adding of N, N'-diisopropylethylamine (DIPEA, 1.5 mL, 8.5 mmol), the reaction mixture was stirred at the same temperature for 24 hours. After that, the solvent was removed under reduced pressure and the mixture was diluted with a saturated solution of NaHCO₃ (40 mL) and extracted with dichloromethane (3×40 mL). The extracted organic layer was dried over anhydrous Na₂SO₄ and evaporated under reduced pressure. The crude product was purified by silica gel column chromatography using 10% Methanol-Dichloromethane as the eluent, to afford ABL-His-NHBoc **9** as a white solid (1.69 g, 50%). ¹H NMR (400 MHz, CDCl₃), δ 8.13 (s, 1H), 7.91 (s, 1H), 7.35 (s, 1H), 6.95 (s, 1H), 4.45 – 4.35 (m, 2H), 3.45 – 3.25 (m, 2H), 3.19 – 3.00 (m, 3H), 2.26 – 2.06 (m, 2H), 1.67 – 1.52 (m, 2H), 1.41 (s, 9H), 1.34 - 1.18 (m, 12H), 0.87 (t, J = 6.8 Hz, 3H).

Synthesis of *N*-(2-(2-amino-3-(1H-imidazol-4-yl)propanamido)ethyl)decanamide (ABL-His-NH₂, 10)

In a dry flask equipped with a stirring bar, the ABL-His-NHBoc (600 mg, 1.33 mmol) was dissolved in 1:1 v/v mixture of TFA/DCM (6 mL) and allowed to stir at room temperature for 5 hours. The reaction was monitored via TLC. Upon complete conversion of the N-Boc-protected amine, saturated NaHCO₃ (30 mL)

was added to the resulting solution and the whole was extracted with dichloromethane (30×3 mL). Combined organic extracts were dried over Na₂SO₄ and concentrated to give the ABL-His-NH₂ (325 mg, 70 %) as clear oil. ¹H NMR (400 MHz, CDCl₃), δ 8.89 (s, 1H), 7.45 (s, 1H), 6.95 (s, 1H), 4.12 (t, J = 6.2 Hz, 2H), 3.34 – 3.30 (m, 5H), 3.12 - 3.06 (m, 3H), 2.26 – 2.06 (m, 2H), 1.67 – 1.52 (m, 2H), 1.26 – 1.18 (m, 12H), 0.89 (t, J = 5.5 Hz, 3H).

Synthesis of *tert*-butyl (2-((2-decanamidoethyl)amino)-2-oxoethyl)carbamate (ABL-Gly-NHBoc, 9')

A mixture of ABL-NH₂ (338 mg, 1.58 mmol), N-(*tert*-Butoxycarbonyl)-glycine (276 mg, 1.57 mmol), and benzotriazol-1-yloxytris(dimethylamino)phosphonium hexafluorophosphate (BOP, 698 mg, 1.57 mmol) in anhydrous dichloromethane (DCM, 40 mL) was stirred at room temperature for 30 minutes. After adding of N, N'-diisopropylethylamine (0.63 mL, 3.63 mmol), the reaction mixture was stirred at the same temperature for 18 hours. After that, the solvent was removed and the mixture was diluted with a saturated solution of NaHCO₃ (50 mL) and extracted with dichloromethane (3×50 mL). The mixture was dried and evaporated under reduced pressure. The crude product was purified by silica gel column chromatography using 10% Methanol-Dichloromethane as the eluent, to afford ABL-Gly-NHBoc as a white solid (316 mg, 86%). ¹H NMR (400 MHz, CDCl₃), δ 6.77 (s, 1H), 6.17 (s, 1H), 5.15 (s, 1H), 3.38 – 3.32 (m, 2H), 3.30 – 3.22 (m, 2H), 2.20 – 2.12 (m, 2H), 1.67 – 1.52 (m, 2H), 1.41 (s, 9H), 1.32 – 1.21 (m, 12H), 0.87 (t, J = 6.9 Hz, 3H).

Synthesis of N-(2-(2-aminoacetamido)ethyl)decanamide (ABL-Gly-NH₂, 10')

In a dry flask equipped with a stirring bar, the ABL-Gly-NHBoc **9'** (120 mg, 0.33 mmol) was dissolved in 1:1 v/v mixture of TFA/DCM (3 mL) and allowed to stir at room temperature for 5 hours. Upon complete conversion of the N-Boc-protected amine, the whole was concentrated to give the ABL-Gly-NH₂ (116 mg, 99%) as clear oil. ¹H NMR (400 MHz, CDCl₃), δ 7.88 (s, 1H), 6.96 (s, 1H), 3.60 – 3.52(m, 2H), 3.26 – 3.22 (m, 4H), 2.28 – 2.21 (m, 2H), 1.57 – 1.53 (m, 2H), 1.25 – 1.19 (m, 12H), 0.87 (t, J = 6.8 Hz, 3H).

Synthesis of N-(9-(2-carboxy-4-(3-(1-((2-decanamidoethyl)amino)-3-(1H-imidazol-4-yl)-1-oxopropan-2-yl)thioureido)phenyl)-6-(diethylamino)-3H-xanthen-3-ylidene)-N-ethylethanaminium (RITC-ABL-His, 1)

A mixture of ABL-His-NH₂ (50 mg, 0.014 mmol) and Rhodamine B isothiocyanate (114 mg, 0.021 mmol) in anhydrous N, N-dimethylformamide (DMF, 1.5 mL) was stirred and heated at 80 °C in a heating block for 1 hour. After cooling to ambient temperature, the reaction mixture was purified by HPLC system (Agilent, Xterra RP-C18 column, 7 μm, 21.2 × 250 mm; 0.1% formic acid in acetonitrile : 0.1% formic acid in deionized water, λ = 254 nm, flow rate= 6.0 mL/min).

Synthesis of N-(9-(2-carboxy-4-(3-(2-((2-decanamidoethyl)amino)-2-oxoethyl)thioureido)phenyl)-6-(diethylamino)-3H-xanthen-3-ylidene)-N-ethylethanaminium (RITC-ABL-Gly, 2)

A mixture of ABL-Gly-NH₂ (21.5 mg, 0.084 mmol) and Rhodamine B isothiocyanate (RITC, 114 mg, 0.125 mmol) in anhydrous N, N-dimethylformamide (DMF, 1.5 mL) was stirred and heated at 80 °C in a heating

block for 1 hour. The mixture was purified by HPLC system (Agilent, Xterra RP-C18 column, 7 μm , 21.2 \times 250 mm; 0.1% formic acid in acetonitrile : 0.1% formic acid in deionized water, $\lambda = 254 \text{ nm}$, flow rate= 6.0 mL/min).

2.3 Synthesis of IR780-ABLs

Synthesis of 2-((E)-2-((E)-4'-amino-6-(2-((E)-3,3-dimethyl-1-propylindolin-2-ylidene)ethylidene)-3,4,5,6-tetrahydro-[1,1'-biphenyl]-2-yl)vinyl)-3,3-dimethyl-1-propyl-3H-indol-1-ium iodide (IR780-NH₂)

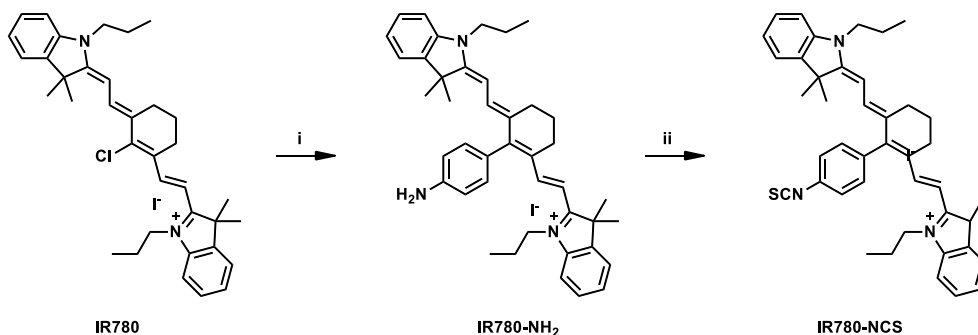


Figure 2.2 Synthesis of IR780-NCS. Reagent and conditions: (i) 4-aminothiophenol, DMF, 25 °C, 24 h; (ii) di(2-pyridyl)thionocarbonate, DCM, 25 °C, 12h.

IR780 (500 mg, 0.75 mmol) was dissolved in 10 mL N, N-dimethylformamide, along with 4-aminothiophenol (186 mg, 1.49 mmol). The reaction mixture was stirred at room temperature at 24 h. The N, N-dimethylformamide was removed and the crude product was purified by silica gel column chromatography using 10% Methanol-Dichloromethane as the eluent, to afford IR780-NH₂ as a dark green solid (443 g, 89%); ¹H NMR (400 MHz, MeOD) δ 1.04 (t, $J = 7.2 \text{ Hz}$, 6H), 1.57 (s, 12H), 1.82 - 1.92 (m, 4H), 1.96 - 2.04 (m, 2H), 2.74 (t, $J = 7.0 \text{ Hz}$, 4H), 4.11 (t, $J = 7.6 \text{ Hz}$, 4H), 6.28 (d, $J = 14.0 \text{ Hz}$, 2H), 6.64 (d, $J = 8.8 \text{ Hz}$, 2H), 7.02

(d, $J = 8.8$ Hz, 2H), 7.20 - 7.32 (m, 4H), 7.38 - 7.49 (m, 4H), 8.86 (d, $J = 10.0$ Hz, 2H); MS (ESI) m/z 628.4 (M-I)⁺.

Synthesis of 2-((E)-2-((E)-6-(2-((E)-3,3-dimethyl-1-propylindolin-2-ylidene)ethylidene)-4'-isothiocyanato-3,4,5,6-tetrahydro-[1,1'-biphenyl]-2-yl)vinyl)-3-methyl-1-propyl-3H-indol-1-ium (IR780-NCS)

The solution of di(2-pyridyl)thionocarbonate (23 mg, 0.099 mmol) in N, N-dimethylformamide (5 mL) was added dropwise to a stirred solution of IR780-NH₂, (50 mg, 0.066 mmol) in N, N-dimethylformamide (1 mL), and the mixture was stirred at room temperature for 12 h. After the reaction, the solvent was removed and then mixture was dissolved in 1 mL of dichloromethane. The crude mixture was added dropwise to cold diethyl ether (10 mL) and kept at -20 °C for 2 h three times. After centrifuging (3400 rpm, 12 min), the supernatant was removed and solid was isolated. The solid was dried under reduced pressure to afford IR780-NCS as a deep dark solid (44.5 mg, 88%).

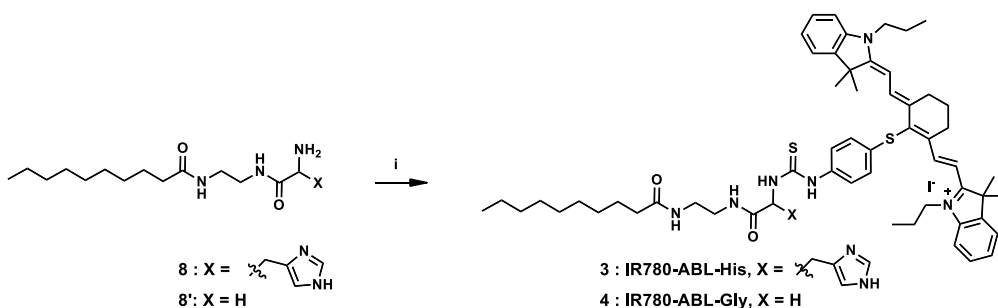


Figure 2.3 Synthesis of IR780-ABL-His (3) and IR780-ABL-Gly (4). Reagent and conditions: (i) IR780-NCS, TEA, DMF, 85 °C, 1 h

Synthesis of 2-((E)-2-((E)-2-((4-(3-(1-((2-decanamidoethyl)amino)-3-(1H-imidazol-4-yl)-1-oxopropan-2-yl)thioureido)phenyl)thio)-3-(2-((E)-3,3-dimethyl-1-propylindolin-2-ylidene)ethylidene)cyclohex-1-en-1-yl)vinyl)-3,3-dimethyl-1-propyl-3H-indol-1-ium (IR780-ABL-His, 3)

ABL-His-NH₂ **8** (50 mg, 0.14 mmol) was dissolved in solution of 1 mL N, N-dimethylformamide and TEA(0.03 mL, 0.23 mmol) in a 4 mL vial. IR780-NCS (47mg, 0.071 mmol) was added, the reaction mixture was stirred at 85 °C for 1 h. After 24 h stirring, the N, N-dimethylformamide was removed under reduced pressure and 1 mL of dichloromethane was added to dissolve crude mixture. The crude mixture in dichloromethane was added dropwise to cold diethyl ether (10 mL) and kept at -20 °C for 2 h three times. After centrifuging (3400 rpm, 15 min), solid was isolated and dried under reduced pressure to afford IR780-ABL-His **3** as a deep dark solid (61.7 mg, 76%).

Synthesis of 2-((E)-2-((E)-2-((4-(3-(2-((2-decanamidoethyl)amino)-2-oxoethyl)thioureido)phenyl)thio)-3-(2-((E)-3,3-dimethyl-1-propylindolin-2-ylidene)ethylidene)cyclohex-1-en-1-yl)vinyl)-3,3-dimethyl-1-propyl-3H-indol-1-ium iodide (IR780-ABL-Gly, 4)

ABL-Gly-NH₂ **8'** (18.7 mg, 0.055 mmol) was dissolved in solution of 1 mL N, N-dimethylformamide and TEA (0.03 mL, 0.165 mmol) in a 4 mL vial. IR780-NCS (67 mg, 0.11mmol) was added, the reaction mixture was stirred at **85 °C for 1 h**. After 24 h stirring, the N, N-dimethylformamide was removed under reduced pressure and 1 mL of dichloromethane was added to dissolve crude mixture. The mixture solution in dichloromethane was added dropwise to cold diethyl ether (10 mL) and kept at -20 °C for 2 h three times. After centrifuging (3400 rpm, 15 min),

solid was isolated and dried under reduced pressure to afford IR780-ABL-Gly **4** as a deep dark solid (36 mg, 49%).

2.4 Synthesis of [⁶⁴Cu]DOTA-ABLs

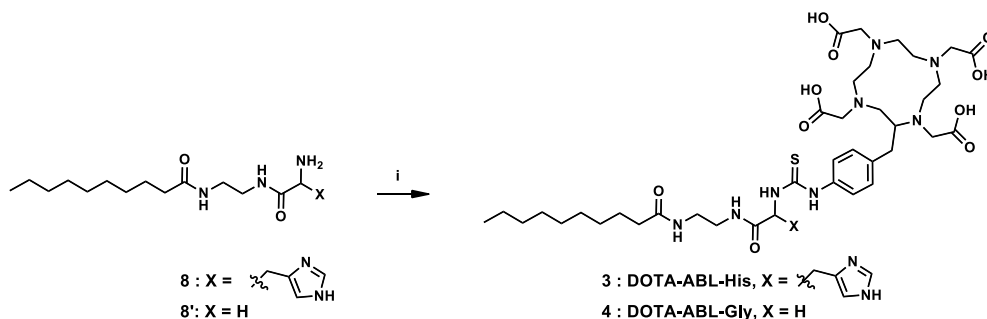


Figure 2.4 Synthesis of DOTA-ABL-His (5') and DOTA-ABL-Gly (6'). Reagent and conditions: (i) (p-SCN-Bn)-DOTA, TEA, DMF, 85 °C, 1 h

Synthesis of 2,2',2'',2'''-(2-(4-(3-(1-((2-decanamidoethyl)amino)-3-(1H-imidazol-4-yl)-1-oxopropan-2-yl)thioureido)benzyl)-1,4,7,10-tetraazacyclododecane-1,4,7,10-tetrayl)tetraacetic acid (DOTA-ABL-His, 5')

ABL-His-NH₂ **10** (20 mg, 0.056 mmol) was dissolved in solution of 1 mL N, N-dimethylformamide and TEA(0.03 mL, 0.23 mmol) in a 4 mL vial. (p-SCN-Bn)-DOTA (50 mg, 0.072 mmol) was added, the reaction mixture was stirred at 85 °C for 1 h. After 24 h stirring, the N, N-dimethylformamide was removed under reduced pressure. The crude mixture was purified by HPLC system (Agilent, Xterra RP-C18 column, 7 μm, 21.2 x 250 mm; 0.1% formic acid in acetonitrile : 0.1% formic acid in deionized water, λ = 254 nm, flow rate= 6.0 mL/min).

Synthesis of 2,2',2'',2'''-(2-(4-(3-(2-((2-decanamidoethyl)amino)-2-

oxoethyl)thioureido)benzyl)-1,4,7,10-tetraazacyclododecane-1,4,7,10-tetrayl)tetraacetic acid (DOTA-ABL-Gly, 6')

ABL-Gly-NH₂ **10'** (50 mg, 0.14 mmol) was dissolved in solution of 1 mL N, N-dimethylformamide and TEA (0.03 mL, 0.23 mmol) in a 4 mL vial. (p-SCN-Bn)-DOTA (50 mg, 0.072 mmol) was added, the reaction mixture was stirred at 85 °C for 1 h. After 24 h stirring, the N, N-dimethylformamide was removed under reduced pressure. The crude mixture was purified by HPLC system (Agilent, Xterra RP-C18 column, 7 μm, 21.2 × 250 mm; 0.1% formic acid in acetonitrile : 0.1% formic acid in deionized water, λ = 254 nm, flow rate= 6.0 mL/min).

Radiosynthesis of 2,2',2'',2'''-(2-(4-(3-(1-((2-decanamidoethyl)amino)-3-(1H-imidazol-4-yl)-1-oxopropan-2-yl)thioureido)benzyl)-1,4,7,10-tetraazacyclododecane-1,4,7,10-tetrayl)tetraacetic acid ([⁶⁴Cu]DOTA-ABL-His, 5)

To a solution of DOTA-ABL-His **5'** was dissolved in 1 mL of water in a 4 mL vial, [⁶⁴Cu]CuCl₂ was added. The reaction mixture was stirred at 80 °C for 1 h and kept at room temperature. This solution was loaded into a tC18 Sep-Pak cartridge, washed with water (10 mL), and eluted with ethanol (0.7 mL). Result solution was dried by azeotropic distillation under a stream of nitrogen gas. Then 10% ethanol-saline solution was prepared for the preclinical studies

Radiosynthesis of 2,2',2'',2'''-(2-(4-(3-(2-((2-decanamidoethyl)amino)-2-oxoethyl)thioureido)benzyl)-1,4,7,10-tetraazacyclododecane-1,4,7,10-tetrayl)tetraacetic acid ([⁶⁴Cu]DOTA-ABL-Gly, 6)

To a solution of DOTA-ABL-Gly **6'** was dissolved in 1 mL of water in a 4 mL

μM of final concentration to observe optical properties of the RITC-ABLs. Fluorescence solution at the aimed concentrations was incubated in a 96-well plate to measure optical properties of the RITC-ABLs. A microplate reader (SYNERGY H1, BioTek, Winooski, VT, USA) was utilized to record absorbance within 230-980 nm range and fluorescence emission spectra from 300 nm to 700 nm at 5nm break. λ_{Abs} and λ_{Em} value of fluorescences were confirmed and fluorescence intensity was obtained by using the microplate reader as well.

Molecular docking study

A 2D model of RITC, RITC-ABL-Gly, and RITC-ABL-His was created using Chemdraw software (version 12.0). The number of ligand molecules was transformed to 3D in Schrodinger Suite (version Maestro 12.5) using the 3D builder tool. As receptors, we employed bovine serum albumin and human serum albumin proteins and Both proteins' pdb files were obtained from the Protein Data Bank service. The pdb ID for BSA is 4F5S, whereas the pdb ID for HSA is 3JRY.

The Glide Maestro (version 12.5) program was used to estimate binding affinities, ligand efficiency, and inhibitory constants for the target using extra-precision docking parameters. All of the ligands were docked with the target's active site using Glide standard precision (SP) mode, which docks to determine the ligands' flexibility. The active ligand molecules will have accessible postures that will allow them to avoid these penalties while simultaneously receiving positive docking scores.

For validation of binding site, the sitemap building procedure thoroughly examined the protein inner and surface area. Based on the site score and volume area, we picked only one binding site from the target. Following that, a suitable

place for grid generation was selected. To build the grid, we utilized the Schrodinger suite's grid-based ligand docking approach to establish the docking parameters. The target centroid for fixing the ligand binding site is chosen based on the grid output. A rectangle was used to generate the grid box and was defined as a 10-radius radius surrounding the ligand-binding site of the target.

Binding efficacy of RITC-ABLs with serum albumin

To investigate the albumin binding profile, 5 mg BSA/1 mL 1X phosphate buffer saline solution was prepared. After that, excess molar ratio of RITC labeled ABLs was incubated with the albumin solution at 37 °C with stirring to examine binding properties of the ligands. After 30 minutes of incubation, RITC-ABLs with BSA solution was purified by using PD-10 column (GE Healthcare Life Science, Buckinghamshire, UK) packed with Sephadex™ G-25M for size exclusion chromatography to remove unbound molecules from the protein. Fluorescence intensity of purified albumin solution was measured to determine percentage fluorescence intensity (F.I) among RITC-ABL-His, RITC-ABL-Gly and RITC.

$$\text{Percent fluorescence intensity (\%)} = F.I_{\text{protein}}/F.I_{\text{total}} * 100$$

We defined percent fluorescence intensity as binding efficacy of each samples. To quantify the ratio of albumin-ligand complex to whole albumin, we used quantitative fluorescence calibration.

Comparison of albumin binding efficacy between the RITC-ABL-His

and RITC-ABL-Gly under different pH conditions

Binding efficacy of RITC-ABL-His, RITC-ABL-Gly and RITC in acidic condition and neutral condition to evaluate pH-dependent changes in binding efficacy of RITC-ABLs in pH 7.4, 6.5, and 5.5. 5 mg BSA/1 mL 1X phosphate buffer saline solutions in different pH level was prepared. pH buffer solution was p

After that, excess molar ratio of RITC labeled ABLs was incubated with the albumin solution at 37 °C with stirring to examine binding properties of the ligands. After 30 minutes of incubation, the RITC-ABLs with BSA solution was purified by using PD-10 column (GE Healthcare Life Science, Buckinghamshire, UK) packed with Sephadex™ G-25M for size exclusion chromatography to remove unbound molecules from the protein. Fluorescence intensity of purified albumin solution was measured to determine percentage fluorescence intensity among RITC-ABL-His, RITC-ABL-Gly and RITC.

$$\text{Percent fluorescence intensity (\%)} = \text{F.I}_{\text{protein}} / \text{F.I}_{\text{total}} * 100$$

We defined percent fluorescence intensity as binding efficacy of each samples. To quantify the ratio of albumin-ligand complex to whole albumin, we used quantitative fluorescence calibration.

Cellular uptake of RITC-ABL-His and RITC-ABL-Gly imaging

CT26 cells were seeded on confocal dishes overnight at 37 °C under 5% CO₂. To examine the in vitro cellular uptake, 1 mg of RITC-labeled ABLs and free RITC were dissolved in 100 µL of DMSO and diluted with deionized water to the final concentration of 15 µmol/1 mL. After fluorescence probes were added to the

culture medium, the cells were incubated for various time points (0 h, 1.5 h, 12 h, 24 h) and then washed with medium three times. Nuclei and cytoskeleton were co-stained with 10 μ M of Hoechst 33342 (Invitrogen) and ViaFluor[®] 488 respectively. After 30 minutes incubation, the confocal dishes were washed with medium three times. The cellular uptake of each RITC, RITC-ABL-His and RITC-ABL-Gly were observed by confocal microscopy with a 544 nm laser excitation and the fluorescence was collected at wavelengths of 570 nm.

2.5 In vivo/ex vivo evaluation of RITC-ABLs

Murine colon carcinoma xenograft mouse model

All animal experimental designs and protocols were approved by the Institutional Animal Care and Use Committee, Woojung Bio Inc (Approval number: IACUC2003-036-01). CT26 tumor bearing mouse models were prepared for in vivo tumor targeted imaging. All mice were housed in specific pathogen free (SPF) facility. Six-week-aged female BALB/c nude mice (Orient Bio, Seongnam, Korea) were utilized for in vivo imaging. For implantation, CT26 cell line (1×10^5 cells/20 μ L PBS) were subcutaneously injected into the left thigh while the mice were ethically euthanized under anesthesia with isoflurane. Tumor diameter was monitored weekly, and in vivo fluorescence imaging was conducted when the volume of implanted tumor reached 200-300 mm³.

In vivo fluorescence imaging with RITC- labeled ABL-His and ABL-Gly

The different four 6-week-old CT26 tumor xenografts were used for IVIS

fluorescence imaging. Three weeks after CT26 cell transplantation, three samples including RITC-ABL-His, RITC-ABL-Gly and RITC (### M, 50 μ L) were injected to the CT26 tumor bearing mice intravenously through the tail vein (n=4). In vivo images were obtained at different time points (0, 2, 8, and 24 h) from the injection using IVIS. After in vivo imaging, the mice were sacrificed and their organs to be evaluated were extracted. Tumor and five major organs including heart, lung, liver, spleen, kidneys were collected and then ex vivo imaging was conducted. To quantify the fluorescence signal, regions of interest (ROI) values were defined and measured and analyzed for the tumor regions and collected organs (heart, lung, liver, spleen, kidney) with fluorescence images by using Living images[®] software (version 4.7.3) for quantitative analysis. After that, each tumor to main organs was analyzed statistically.

Statistics

Statistical analysis was carried out using MedCalc[®] for Windows (MedCalc software, Mariakerke, Belgium). All quantitative values were presented as mean \pm standard deviation (SD). The means were compared among three groups using the One-way analysis of variance (ANOVA). Unpaired Student's t-test were performed to assess differences between the two data sets, which is pH-responsive profile of the RITC-ABL-His and RITC-ABL-Gly bound to BSA. P-values less than 0.05 were considered statistically significant. Data from ex vivo imaging including biodistribution analyses were collected from 4 mice for each probe. All the In vitro and in vivo data was evaluated within SigmaPlot and ANOVA analysis, $p < 0.05$ was considered statistically significant.

Chapter 3. Result and discussion

3.1 Chemistry of the albumin binding ligands.

Synthesis of the albumin binding ligands

The key precursor (8), utilized to prepare RITC-labeled albumin binding ligand described, was synthesized by 4 step synthesis using tert-butyl (2-aminoethyl)carbamate as a starting compound. Compound (5) was obtained by means of amide condensation from the starting material with decanoic acid in a DCM mixture at room temperature. After deprotecting of Boc group in compound (5), N-(2-aminoethyl)decanamide (6) was conjugated with (2S)-3-(1H-imidazol-5-yl)-2-[(2-methylpropan-2-yl)oxycarbonylamino]propanoic acid to gain compound to gain compound (7) and N-tert-butoxycarbonyl-glycine was introduced to synthesized compound (7') as a control group for pH sensitivity. For this reason, the reaction of ABL-His and ABL-Gly with RITC was respectively prepared. Each compound (8) and (8') was labeled with Rhodamine B in same reaction condition as depicted in **(Figure 2.1)**. Synthesized RITC-ABL-His (1) and RITC-ABL-Gly (2) were purified and characterized by high performance liquid chromatography and mass spectrum.

In a same fashion, IR780 was modified with 4-aminothiophenol which is thiol linker by substitution of meso-Cl in IR780 to give IR780-NH₂ by same condition that was shown in the literature [37]. Finally, the compound (10) and (10') was conjugated with modified IR780 to give the compound IR780-ABL-His (3) and the compound IR780-ABL-Gly (4). The obtained IR780-conjugated ABLs were clearly washed with cold ether. Physicochemical properties of IR780-ABL-His and IR780-ABL-Gly were under investigated for the photodynamic therapy and

imaging.

In case of the DOTA-ABLs, the compound (8) and (8') was conjugated with DOTA moiety to give the compound DOTA-ABL-His (5') and the compound DOTA-ABL-Gly (6'). The obtained DOTA-conjugated ABL were purified by HPLC system and Cu-64 was labeled for cancer targeted nuclear imaging and radionuclide therapy.

Characterization of the RITC-ABLs

As fluorescence of the RITC-ABLs is derived from the RITC structure, optical properties of RITC-ABL-His and RITC-ABL-Gly were similar to those of RITC. The absorbance maxima and emission maxima were obtained at around 550 nm and 570 nm respectively, which is similar to that of RITC (**Figure 3.1A and B**).

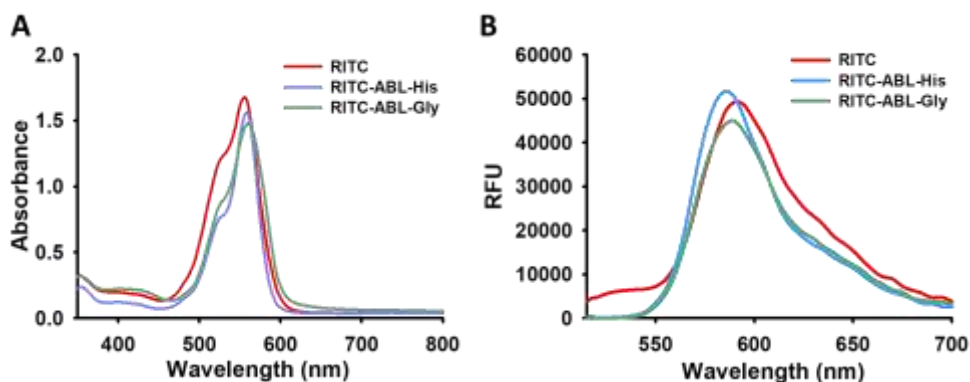


Figure 4.1 (A) UV/Vis absorption spectra and (B) emission spectra of RITC-ABL-His, RITC-ABL-Gly and RITC (Each 1.6 μ M). Similar absorption and emission properties among three molecules was confirmed to have similar absorption maxima at $\lambda \approx 550$ nm and emission maxima at $\lambda \approx 570$ nm.

Molecular docking study

The ligand-target interactions are demonstrated by molecular docking studies, and ligand efficiency contains docking score, electrostatic energy, and hydrogen bond interaction (both side and back chain). In all, three ligand molecules including RITC-ABL-His, RITC-ABL-Gly and RITC were chosen for this docking against the target of two receptors under condition of pH 7.4, 6.5, 5.5. Representative docking simulation of RITC-ABL-His with HSA under three different pH conditions were shown to confirm the protonation effect of imidazole moiety on the ligand in **Figure 3.2**. The bond at pH 6.5 is more than that of pH 5.5. In addition, RITC-ABL-His have the greatest interaction with the protein under pH 7.4 among three pH conditions. Likewise, BSA yields the same outcome as HSA. Those photos clearly illustrate that RITC-ABL-His has a stronger binding affinity at higher pH than at lower pH.

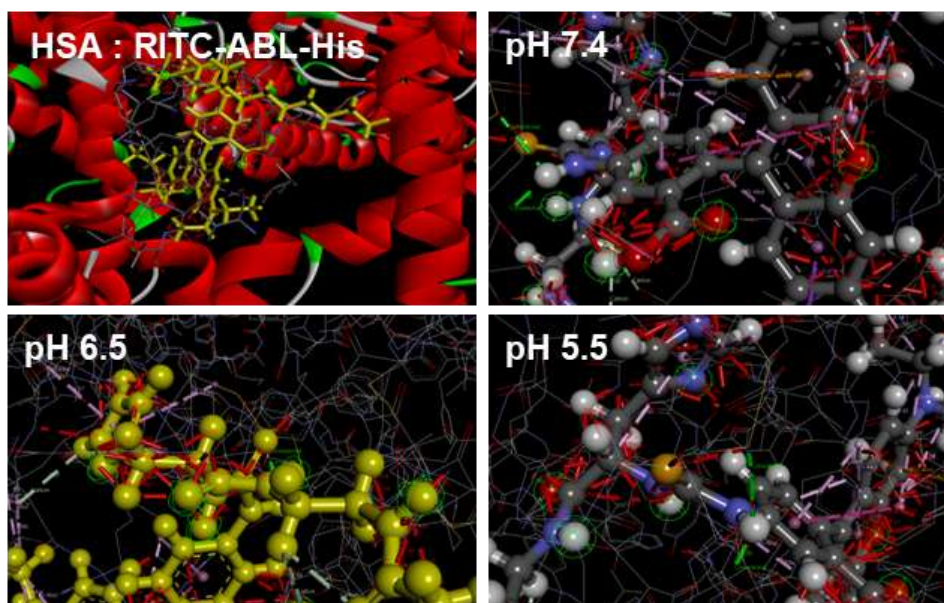


Figure 3.2 Molecular docking simulation of RITC-ABL-His with human serum

albumin under different pH level (pH 7.4, 6.5 and 5.5). It demonstrates the interaction between RITC-ABL-His and HSA. Hydrogen bond (green), covalent bond (pink), and non-covalent bond (Red).

Dockings are often mediated by a variety of inter-atomic interactions, particularly electrostatic energy and Van der Wall forces. Furthermore, these binding affinities are heavily reliant on other parameters such as entropy, desalvation, and receptor molecule flexibility.

Compound	Target Protein	Binding free energy (DS)		
		pH 7.4	pH 6.5	pH 5.5
RITC-ABL-His	HSA	-9.6 Kcal/mole	-9.3 Kcal/mole	-8.9 Kcal/mole
	BSA	-8.3 Kcal/mole	-8.1 Kcal/mole	-7.8 Kcal/mole

Table 2. Evaluated binding free energy of the RITC-ABL-His under three distinct pH condition (pH 7.4, 6.5 and 5.5)

Binding assay and comparison of pH-sensitivity study of RITC-ABLs

ABL's binding profile with bovine serum albumin was examined by using size exclusion chromatography method and fluorescence intensity measured by microplate reader. It was found that the RITC-ABLs attached to albumin more than twice as much as RITC in neutral pH (**Figure 3.3 A**). And we investigated how much the RITC-ABLs are separated from albumin under acidic condition. As a result, RITC-ABL-His was identified to have reduced binding profile with albumin as the pH decreased from 7.4 to 5.5 (**Figure 3.3 B**) and RITC-ABL-Gly showed no difference in all range of pH. After that, the cellular uptake profile of CT26 cancer cells was observed at neutral pH, and there was no significant difference between

the two ligands. In short, it was considered the ABLs bind to albumin effectively. And in the case of RITC-ABL-His, it was released from albumin at low pH condition. So, in neutral pH, in vitro cellular uptake profile of two ligands was similar.

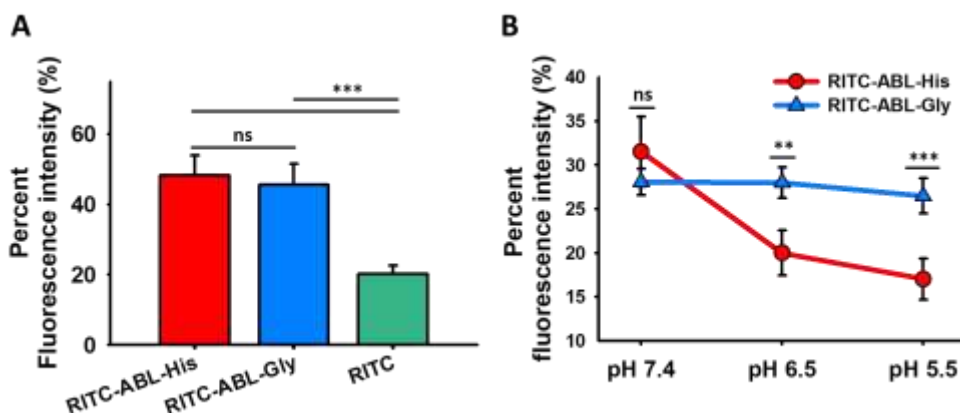


Figure 3.3 (A) Binding profiles with BSA was examined by using size exclusion chromatography method. The RITC-ABLs attached to albumin more than twice as much as free RITC in neutral pH. (B) Released RITC-ABLs from albumin under acidic condition was measured. pH-responsive RITC-ABL-His was identified to have reduced binding efficacy with albumin as the pH decreased from 7.4 to 5.5. RITC-ABL-Gly showed no difference in all range of pH. (ns = not significant $p \geq 0.05$, ** $p < 0.01$, *** $p < 0.001$)

3.2 In vitro imaging and cellular uptake of RITC-ABLs

Cellular uptake of RITC-ABLs in CT26 cell

In order to evaluate in vitro cellular uptake, confocal imaging of RITC-ABL-His and RITC-ABL-Gly were performed in CT26 cancer cells (**Figure 3.4**). There were no difference in confocal imaging of both RITC-ABL (RITC-ABL-His and RITC-

ABL-Gly) in CT26 cells, compared to control (RITC). In vitro confocal imaging suggested that RITC-ABL-His and RITC-ABL-Gly showed similar cellular uptake profile in CT26 cell line under neutral pH condition of cell growth media. In addition, albumin in which the probes bind to and pH condition play vital roles to provide desired functionalities including albumin binding characteristic and pH-sensitivity.

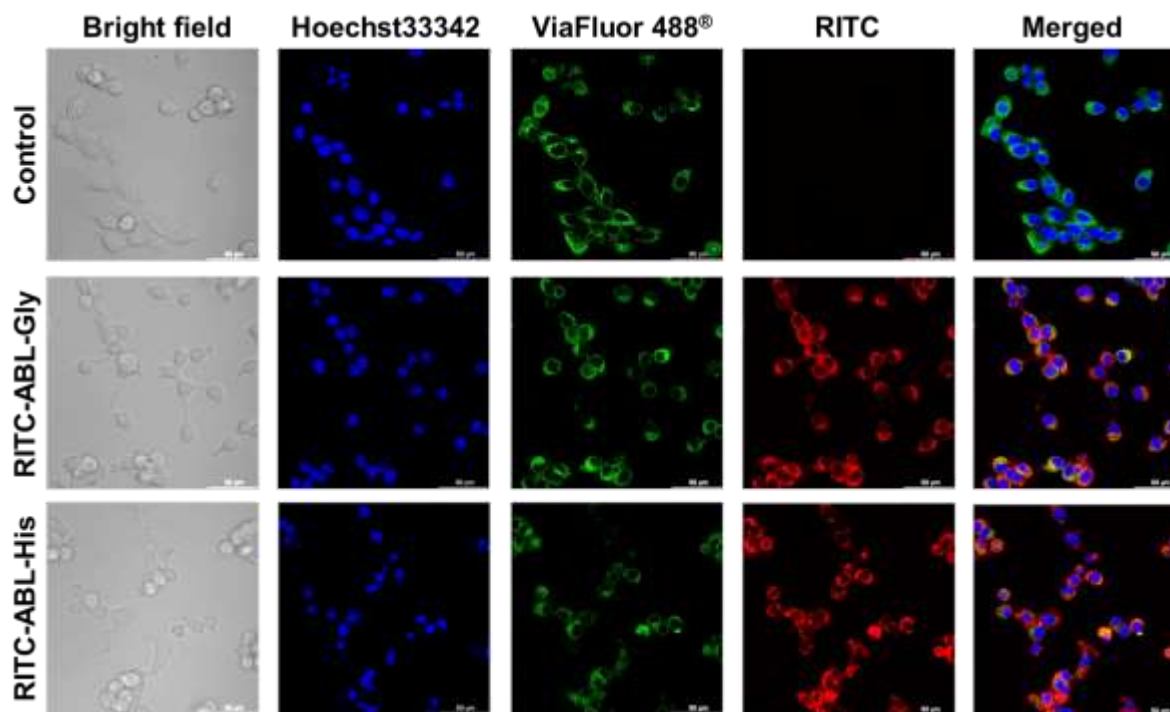


Figure 3.4 In vitro cellular uptake of CT26 cancer cells was observed, 15 μ mol of RITC-ABL-His and RITC-ABL-Gly treated CT26 cells at all the various time points (0, 1.5, 2, 12 and 24 h).

3.3 In vivo and ex vivo optical imaging of the RITC-ABLs

In vivo and ex vivo fluorescence imaging in CT26 tumor bearing mouse model

In order to evaluate circulation and tumor targeting ability, bio-distribution of RITC-ABL, in vivo fluorescence imaging was performed comparing to RITC. Fluorescence imaging was conducted using RITC-ABL-His, RITC-ABL-Gly and RITC at various time point (0, 2, 8, 24 h). Bio-distribution of in vivo optical imaging by Rhodamine B isothiocyanate (RITC) is not accurate to distinguish the signal due to the auto-fluorescence in mouse body (**Figure 3.5 A**). However, blood half-life was enhanced in case of the RITC-ABLs. The intensity of RITC signal showed difference between the RITC-ABLs and free RITC. In case of RITC-ABL-His and RITC-ABL-Gly, their RITC signal was detected higher than free RITC from 2 h to 24 h post injection, and difference of fluorescence intensity increased significantly.

To confirm the distribution of the RITC-ABL-His and RITC-ABL-Gly in CT26 tumor bearing mouse model, tumor and peripheral organs including liver, heart, lung, kidney, spleen were collected after in vivo imaging. In case of RITC-ABL-His, strong RITC signal was found in tumor which suggests that tumor targeting ability was highly superior compared to others (**Figure 3.5 B**). It was also accumulated in liver and kidney as well. In contrast, RITC-ABL-Gly showed reduced tumor uptake, there is no difference in tumor uptake and liver uptake of RITC-ABL-Gly. Distributions of the RITC-ABLs were different, so low tumor accumulation of RITC-ABL-Gly which has no imidazole functional group could be explained. We assume that pH-responsive moiety enhance tumor targeting functionality.

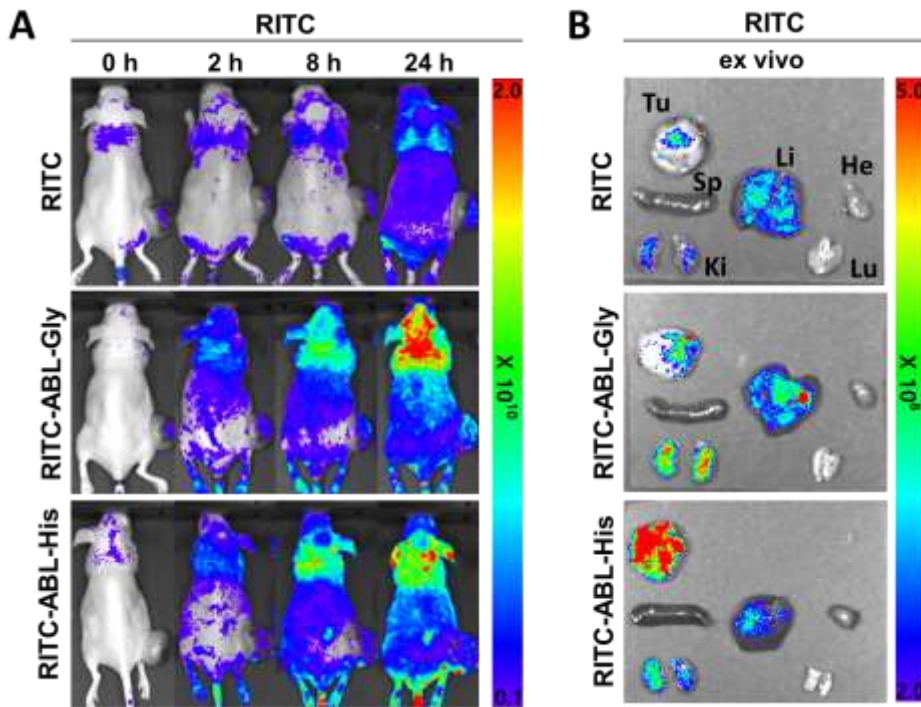


Figure 3.5 Representative in vivo and ex vivo fluorescence images of RITC-ABL-His, RITC-ABL-Gly and RITC in CT26 tumor bearing mouse model at 0, 2, 8, 24 h post injection (n=4). (Tu: tumor, Sp: spleen, Li: liver, He: heart, Ki: kidney, Lu: lung).

Quantitative analysis of tumor and normal organ uptake

Based on ex vivo fluorescence imaging of RITC-ABL-His, RITC-ABL-Gly and RITC in CT26 tumor bearing-mice, fluorescence intensity of tumor and other organs were quantified (**Figure 3.6**). The tumor targeting ability of RITC-ABL-His was twice higher than that of others as RITC-ABL-His group was significantly higher than that of the other two groups (**Figure 3.6 A**). Accumulation of the RITC-ABLs and RITC in five normal organs showed no significant differences, fluorescence intensity of RITC in kidney showed slightly lower value than that of two RITC-ABLs. We assume that fast renal clearance of RITC occurred after injection owing to its absence of albumin binding ability that enhanced blood circulating functionality. In case of RITC-ABL-His, tumor to normal organs including liver, spleen, heart, lung and kidney ratio showed similar result up to 1.89, 13.6, 9.95, 9.78 and 1.79 folds, respectively (**Figure 3.6 B-F**).

Considering these results of in vivo and ex vivo fluorescence imaging, RITC-ABL-His showed outstanding specificity to tumor as a fluorescence probes for tumor delivery that has longer blood circulation via binding ability to albumin and pH-responsive profile in acidic tumor microenvironment.

Interestingly, it is notable that there is no difference in in vitro profiles among RITC-ABL-His, RITC-ABL-Gly and RITC compared to in vivo and ex vivo imaging. We assume that presence of serum albumin in blood stream is one of the most important key factors that makes the RITC-ABL works well, and that it makes significant result in tumor targeting efficacy.

Moreover, it is necessary to dramatically overcome rapid clearance from the body that is one of the general limitations small molecule drugs have by modifying albumin binder part of the ABLs, thereby increasing both active and passive tumor

targeting efficacy of the ABL. Also, replacing imidazole with more pH-responsive moiety in structure of ABLs is needed to further research on an enhancement of the higher tumor targeting functionality than that of single imidazole in RITC-ABL-His.

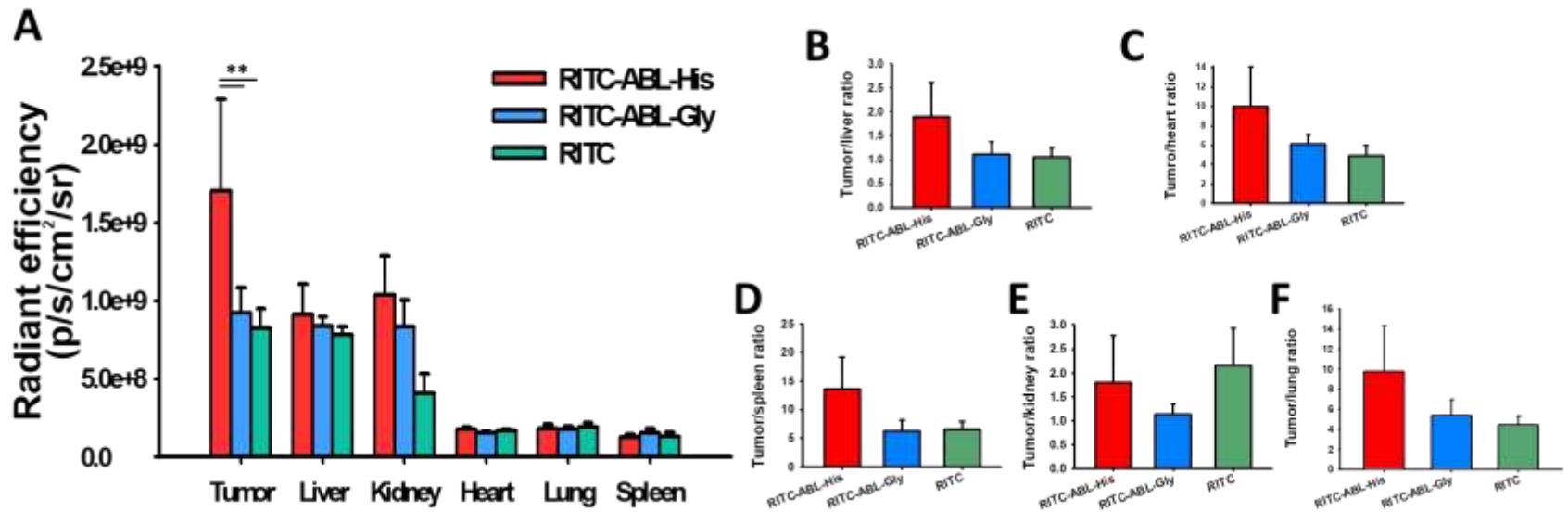


Figure 3.6 Quantitative analysis of ex vivo images of RITC-ABL-His, RITC-ABL-Gly and RITC in CT26 tumor bearing mouse model (n=3) at 24 h after intravenous injection of the fluorescence probes and tumor targeting efficiency compared to five normal organs. (A) Biodistribution analysis of various organs and tumors. (B) Tumor to normal organ ratio (B) liver, (C) heart, (D) spleen, (E) kidney, (F) lung (**p<0.01)

Various application of Albumin binding ligand

The application of ABL-His in areas of cancer targeted therapy would be outstanding value to be further studied by conjugating other therapeutic moieties to provide various capacity for various cancer therapy. That is because most of malignant tumor tissues have acidic microenvironment, so it could be widely used for the solid cancer.

In order to facilitate many types of therapies through using ABL-His as a backbone of potential drug, we conjugated ABL-His to an organic photosensitizer and chelator which can provide functionalities as light/ultrasound-activatable therapy and radionuclide therapy respectively. Enhanced blood circulation and specific uptake in tumors could maximize positive effect in areas of cancer therapy.

In this point, we introduced ABL-His into two different field of cancer therapy. First, we conjugated IR780 derivatives to ABL-His and ALB-Gly to obtain IR780-ABL-His **3** and IR780-ABL-Gly **4**. IR780 is kinds of dye that could work as both photosensitizer and sonosensitizer. Near Infra-Red light (808 nm) and ultrasound activate IR780 to generate ROS (Reactive Oxygen Species) and heat. We designed the IR780-ABLs as a novel organic photodynamic or photothermal therapy agent that could be have therapeutic effect. Special property of photosensitizers is that they have few toxicities without laser irradiation so that it is possible to reduce side effect and increase therapeutic effects on targeted site.

Second one is that the Cu-64 labeled DOTA-ABLs containing DOTA as a chelator for capturing metal or radioisotope. Common disadvantage of radionuclide used for cancer therapy is short rapid clearance from the body. DOTA-ABL-His needs to be further developed and we expected it could overcome general defect and be used widely for radionuclide therapy.

However, there remains for improvement while problems has been solved, ABL-
His has to be optimized.

Chapter 4. Conclusion

In this study, we designed and developed a new type of pH-responsive albumin binding platform which has longer blood half-life and specificity to tumor microenvironment. The development of RITC-labeled new pH-responsive albumin binding ligands showed enormous potential that could be applicable in cancer targeted imaging and therapy. Our strategy to improve pharmacokinetics of tumor targeted probes was to introduce fatty acid as albumin binder in order to provide affinity for serum albumin, by reducing rate of renal clearance which is one of the most important challenges of small molecule-based therapeutics. Studies on albumin binding profile for various usages in drug delivery have been widely reported traditionally.

Considering the result of binding assay with human/bovine serum albumin, RITC-ABL-His and RITC-ABL-Gly showed higher binding efficacy than normal fluorescence dye, RITC.

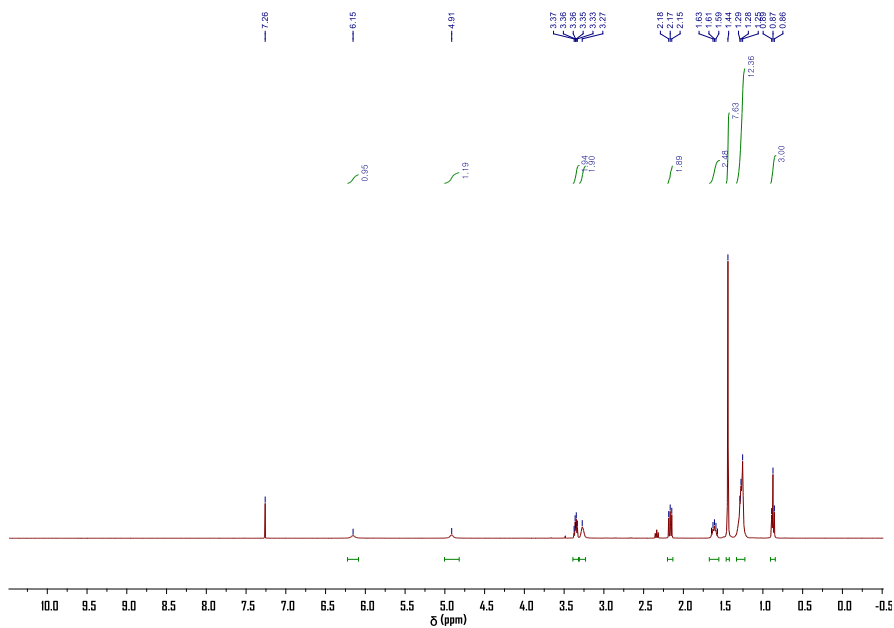
We expect that RITC-ABL-His will be useful tools for in vivo cancer targeted imaging. Also we plan to aid ABL-His to be modified to have better blood half-life as well as pH-sensitivity. Furthermore, a variety of functionalized therapeutic moiety can be introduced to open the door for the outstanding cancer targeted therapy in fields of theranostics which can be result in effective cancer targeted imaging and therapy because most of tumors have acidic condition inside, thereby current clinical technology.

Therefore, we expect that our ligand can be further developed to be cancer therapeutics by immobilizing therapeutic moieties such as radionuclides and photosensitizers.

Appendix

Figure A1. NMR spectra (^1H and ^{13}C NMR) of reported compounds

Synthesis of *tert*-butyl (2-decanamidoethyl)carbamate (ABL-NHBoc, 7)



Synthesis of *N*-(2-aminoethyl)decanamide (ABL-NH₂, 8)

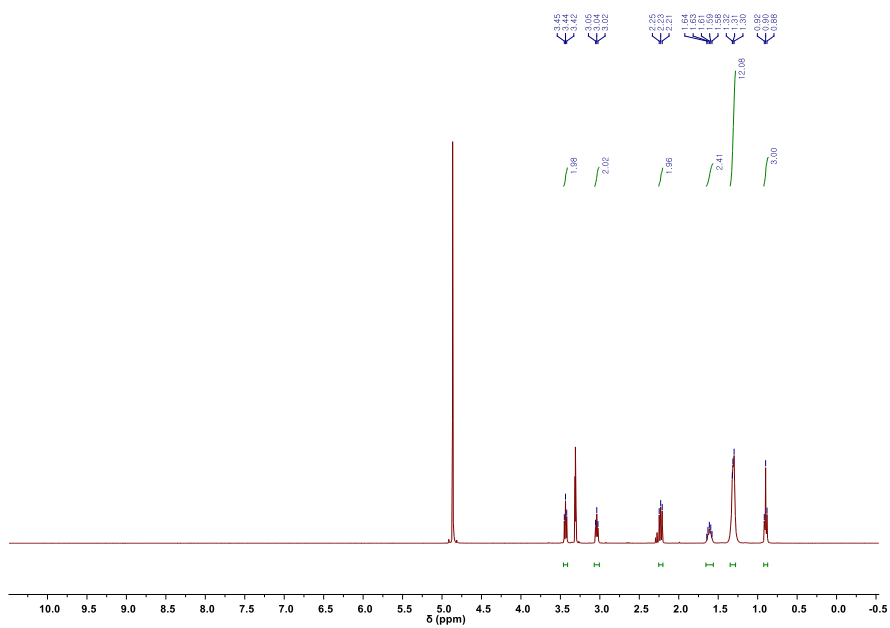
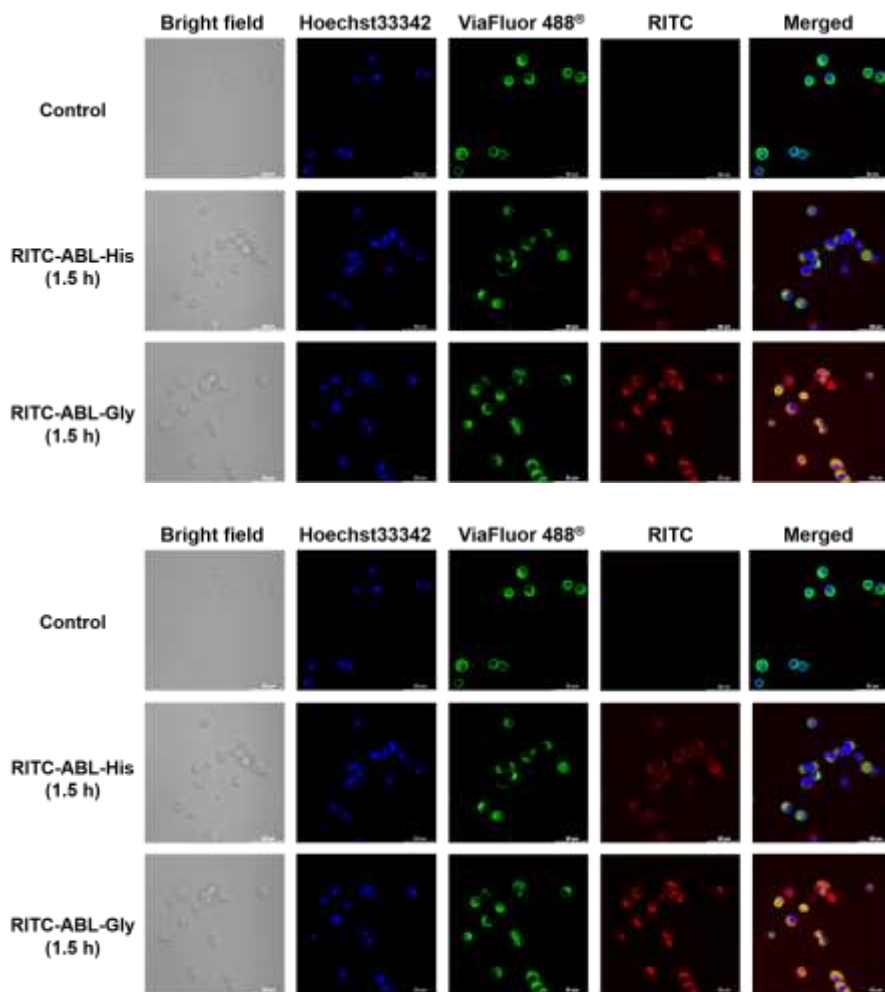


Figure A3. In vitro cellular uptake profile of RITC-ABL-His, RITC-ABL-Gly and RITC (0 h, 1.5h, 24 h)



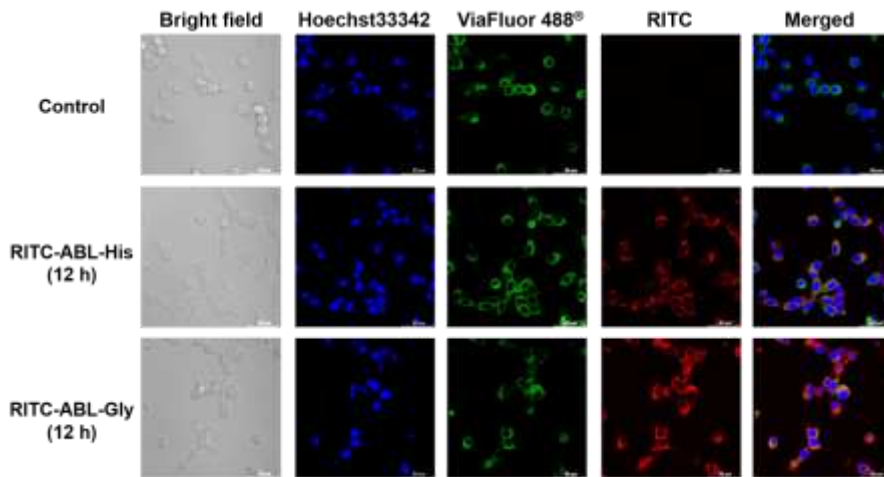


Figure A2. In vivo fluorescence imaging after intravenous injection

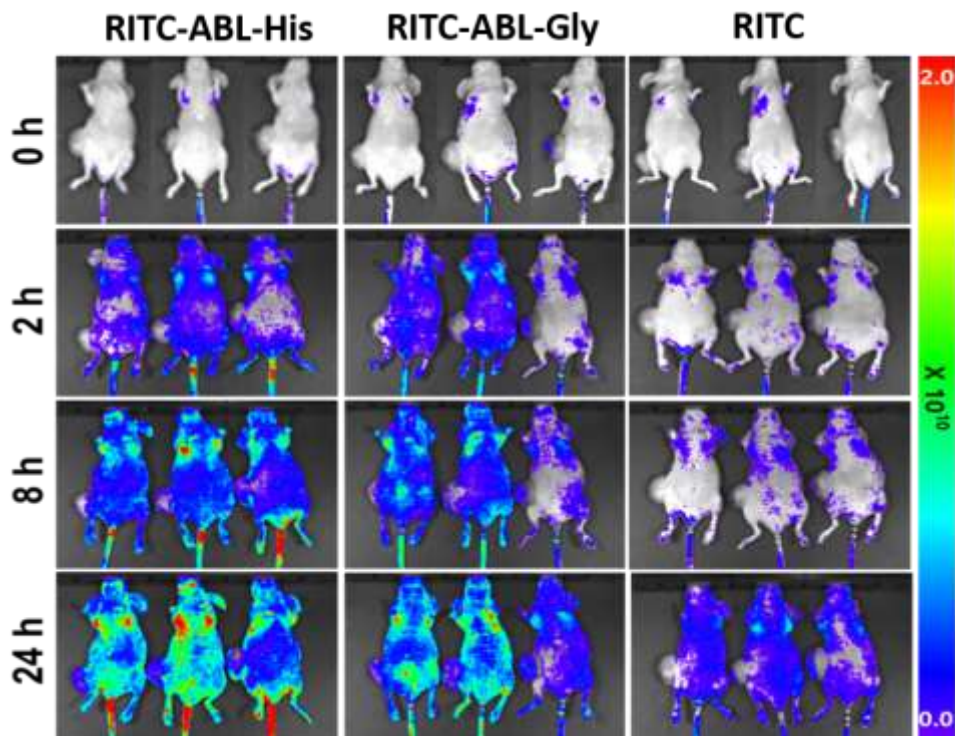
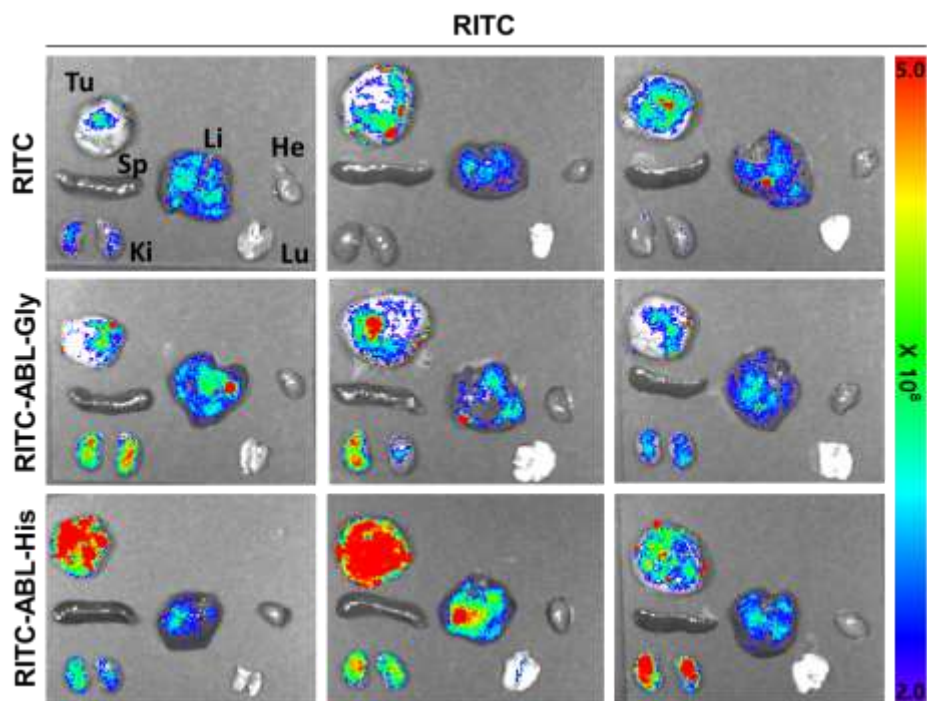


Figure A3. Ex vivo fluorescence images of tumor and non-targeted main organs



Reference

1. Arroyo, V., R. García-Martínez, and X. Salvatella, *Human serum albumin, systemic inflammation, and cirrhosis*. Journal of hepatology, 2014. **61**(2): p. 396-407.
2. Rangan, P. and A. Mondino, *Microbial short-chain fatty acids: a strategy to tune adoptive T cell therapy*. Journal for Immunotherapy of Cancer, 2022. **10**(7).
3. Zorzi, A., S. Linciano, and A. Angelini, *Non-covalent albumin-binding ligands for extending the circulating half-life of small biotherapeutics*. MedChemComm, 2019. **10**(7): p. 1068-1081.
4. Bazban-Shotorbani, S., et al., *Revisiting structure-property relationship of pH-responsive polymers for drug delivery applications*. Journal of Controlled Release, 2017. **253**: p. 46-63.
5. Merlot, A.M., D.S. Kalinowski, and D.R. Richardson, *Unraveling the mysteries of serum albumin—more than just a serum protein*. Frontiers in physiology, 2014. **5**: p. 299.
6. Ishida, T., et al., *New Modalities and Strategies in Drug Delivery and Discovery Foreword*. 2022, PHARMACEUTICAL SOC JAPAN 2-12-15 SHIBUYA, SHIBUYA-KU, TOKYO, 150-0002, JAPAN. p. 309-309.
7. Larsen, M.T., et al., *Albumin-based drug delivery: harnessing nature to cure disease*. Molecular and cellular therapies, 2016. **4**(1): p. 1-12.
8. Peters Jr, T., *All about albumin: biochemistry, genetics, and medical applications*. 1995: Academic press.
9. Fanali, G., et al., *Human serum albumin: from bench to bedside*. Molecular aspects of medicine, 2012. **33**(3): p. 209-290.
10. Kratz, F., *Albumin as a drug carrier: design of prodrugs, drug conjugates and nanoparticles*. Journal of controlled release, 2008. **132**(3): p. 171-183.
11. Mishra, V. and R.J. Heath, *Structural and biochemical features of human serum albumin essential for eukaryotic cell culture*. International Journal of Molecular Sciences, 2021. **22**(16): p. 8411.
12. Linciano, S., et al., *Molecular analysis and therapeutic applications of human serum albumin-fatty acid interactions*. Journal of Controlled Release, 2022. **348**: p. 115-126.
13. Rabbani, G. and S.N. Ahn, *Structure, enzymatic activities, glycation and therapeutic potential of human serum albumin: A natural cargo*. International journal of biological macromolecules, 2019. **123**: p. 979-990.
14. Eldredge, H.B., et al., *Species dependence on plasma protein binding and relaxivity of the gadolinium-based MRI contrast agent MS-325*. Investigative radiology, 2006. **41**(3): p. 229-243.
15. Tian, R., et al., *Evans blue attachment enhances somatostatin receptor subtype-2 imaging and radiotherapy*. Theranostics, 2018. **8**(3): p. 735.
16. Wen, X., et al., *Evans blue-modified radiolabeled fibroblast activation protein inhibitor as long-acting cancer therapeutics*. Theranostics, 2022. **12**(1): p. 422.
17. Cherrick, G.R., et al., *Indocyanine green: observations on its physical properties, plasma decay, and hepatic extraction*. The Journal of clinical investigation, 1960. **39**(4): p. 592-600.
18. Cho, H., et al., *Emerging Albumin-Binding Anticancer Drugs for Tumor-Targeted Drug Delivery: Current Understandings and Clinical Translation*. Pharmaceutics, 2022. **14**(4): p. 728.
19. Elzoghby, A.O., W.M. Samy, and N.A. Elgindy, *Albumin-based nanoparticles as*

- potential controlled release drug delivery systems*. Journal of controlled release, 2012. **157**(2): p. 168-182.
20. Fleury, F., et al., *Camptothecin-binding site in human serum albumin and protein transformations induced by drug binding*. FEBS letters, 1997. **411**(2-3): p. 215-220.
 21. Shen, H., et al., *In vitro study on the binding of gemcitabine to bovine serum albumin*. Journal of pharmaceutical and biomedical analysis, 2013. **75**: p. 86-93.
 22. Dvorak, H.F., *Reconciling VEGF with VPF: the importance of increased vascular permeability for stroma formation in tumors, healing wounds, and chronic inflammation*. Frontiers in Cell and Developmental Biology, 2021. **9**: p. 660609.
 23. Dvorak, H.F., et al., *Vascular permeability factor/vascular endothelial growth factor, microvascular hyperpermeability, and angiogenesis*. The American journal of pathology, 1995. **146**(5): p. 1029.
 24. Fang, J., H. Nakamura, and H. Maeda, *The EPR effect: unique features of tumor blood vessels for drug delivery, factors involved, and limitations and augmentation of the effect*. Advanced drug delivery reviews, 2011. **63**(3): p. 136-151.
 25. Hu, H., et al., *Deciphering albumin-directed drug delivery by imaging*. Advanced Drug Delivery Reviews, 2022: p. 114237.
 26. Hoogenboezem, E.N. and C.L. Duvall, *Harnessing albumin as a carrier for cancer therapies*. Advanced drug delivery reviews, 2018. **130**: p. 73-89.
 27. Larsen, M.T., et al., *FcRn overexpression in human cancer drives albumin recycling and cell growth; a mechanistic basis for exploitation in targeted albumin-drug designs*. Journal of Controlled Release, 2020. **322**: p. 53-63.
 28. Nilsen, J., et al., *Human and mouse albumin bind their respective neonatal Fc receptors differently*. Scientific reports, 2018. **8**(1): p. 1-12.
 29. Chaudhury, C., et al., *The major histocompatibility complex-related Fc receptor for IgG (FcRn) binds albumin and prolongs its lifespan*. Journal of Experimental Medicine, 2003. **197**(3): p. 315-322.
 30. Wakil, S.J. and L.A. Abu-Elheiga, *Fatty acid metabolism: target for metabolic syndrome*. Journal of lipid research, 2009. **50**: p. S138-S143.
 31. Eskew, M.W. and A.S. Benight, *Ligand binding constants for human serum albumin evaluated by ratiometric analysis of DSC thermograms*. Analytical Biochemistry, 2021. **628**: p. 114293.
 32. van Witteloostuijn, S.B., S.L. Pedersen, and K.J. Jensen, *Half-life extension of biopharmaceuticals using chemical methods: alternatives to PEGylation*. ChemMedChem, 2016. **11**(22): p. 2474-2495.
 33. Kim, J.-w. and C.V. Dang, *Cancer's molecular sweet tooth and the Warburg effect*. Cancer research, 2006. **66**(18): p. 8927-8930.
 34. Vaupel, P. *Tumor microenvironmental physiology and its implications for radiation oncology*. in *Seminars in radiation oncology*. 2004. Elsevier.
 35. Zhang, Y., et al., *Intelligent poly (l-histidine)-based nanovehicles for controlled drug delivery*. Journal of Controlled Release, 2022. **349**: p. 963-982.
 36. Dockal, M., D.C. Carter, and F. Rüker, *Conformational transitions of the three recombinant domains of human serum albumin depending on pH*. Journal of Biological Chemistry, 2000. **275**(5): p. 3042-3050.

Abstract in Korean

알부민은 체내 혈장에서 가장 풍부한 단백질 중 하나이며, 최대 19일의 혈중 반감기동안 순환하며 다양한 분자를 수송한다고 알려져 있다. 이러한 알부민의 특성 때문에, 약물에 알부민 결합 모티프를 도입하여 높은 혈중 반감기와 조직 표적능을 향상시킬 수 있다. 본 연구에서는 pH-반응성 지방산 기반 알부민 결합 리간드(ABL-His)를 개발하였고, 이는 알부민과 높은 상호작용을 한다고 알려진 지방산을 기반으로 알부민 결합 모티프와 암 미세환경의 낮은 pH 조건에서 양성자화되어 약물에 특이적인 동향을 부여할 수 있는 이미다졸 작용기로 이루어져 있다. pH-반응성 ABL가 강화된 암 표적능을 갖는 작용 기전은 정맥 주사 후 1) 체내에 순환하며 혈청 알부민에 가역적으로 결합하여 긴 시간동안 체외 배출되지 않고 계속 순환하며 2) 종양 미세환경의 산성조건 내에서 양성자화된 이미다졸로 인해 알부민으로부터 방출되는 능력을 통해 종양 표적 능력이 향상되는 것으로 가정한다. 세포/동물수준에서 암 표적능을 평가하기 위해 ABL에 형광 염료인 Rhodamine B isothiocyanate (RITC)를 도입하였고, 그 결과 효과적인 암표적 추적자로의 잠재력을 확인하였다. 우리는 이미징 및 치료를 위한 ABL의 약물 전달 플랫폼으로서의 높은 잠재력을 제시하고자 한다. 합성한 pH-반응성 중 이미다졸을 포함한 약물을 RITC-ABL-His로 명명하였고, 이에 대한 대조군으로서 이미다졸을 갖고 있지 않는 약물을 RITC-ABL-Gly라고 하였다. 이들의 알부민과의 결합능력을 pH 중성 조건에서 크기 배제 크로마토그래피 방법을 통해 확인하였고, 그 결과 RITC-ABL-His와 -Gly는 형광염료인 RITC(20.2%)에 비해 2배 이상 더 높은 알

부민 결합 능력(각각 48.3, 45.6%)을 나타냈다. 또한 RITC-ABL-His의 경우, 낮은 pH 조건에서 양성자화에 의한 전하 교환 현상으로 인해 pH가 낮아짐에 따라 알부민 결합능이 감소되었다. pH 중성 조건인 CT26 세포 모델에서의 ABL의 세포접착은 높은 형광세기를 보였다. 생체 내/외 형광 영상 촬영을 통해 CT26 암 마우스 모델에서 RITC-ABL-His의 암세포 내 형광 축적 및 세기는 나머지 RITC-ABL-Gly 및 RITC보다 형광 강도가 다른 그룹보다 2배 이상 높음을 확인하였다. 이처럼, RITC가 표지된 ABL의 경우 효과적인 암 표적 이미징 약물로서의 잠재력을 보였으며, 이러한 ABL-His의 뛰어난 암 표적능을 기반으로, ABL에 RITC 대신 근적외선 빛에 활성화되는 광감작제 중 하나인 IR780을 도입하여 IR780-ABL-His를 합성하였다. IR780-ABL-His의 물리화학적 특성은 808 nm의 레이저를 활용한 이미징, 광역학치료 그리고 광열치료제로서 활용할 수 있도록 평가중에 있다. 결과적으로, 알부민과 가역적인 상호작용을 통해 체내 오랜 시간 체류할 수 있고, pH-민감성 작용기를 가져 암세포 등을 선택적으로 표적할 수 있다는 장점을 가지는 ABL은 암 표적 이미징 프로브나 항암치료제의 대단한 잠재력을 가질 수 있을 것으로 기대된다. 이에 더 나아가 방사성 핵종이나 광감작제, 화학요법 약제 등을 ABL-His에 결합시킨다면, 효과적인 암 표적 영상 및 항암약물 플랫폼으로 개발될 수 있기 때문에 이에 대한 범용성을 확장하고자 한다.

주요어 : 알부민, 지방산, pH-반응성, 혈중 반감기, 형광영상

학 번 : 2021-26205